Article

Cell Systems

Biophysics of Temporal Interference Stimulation

Graphical Abstract

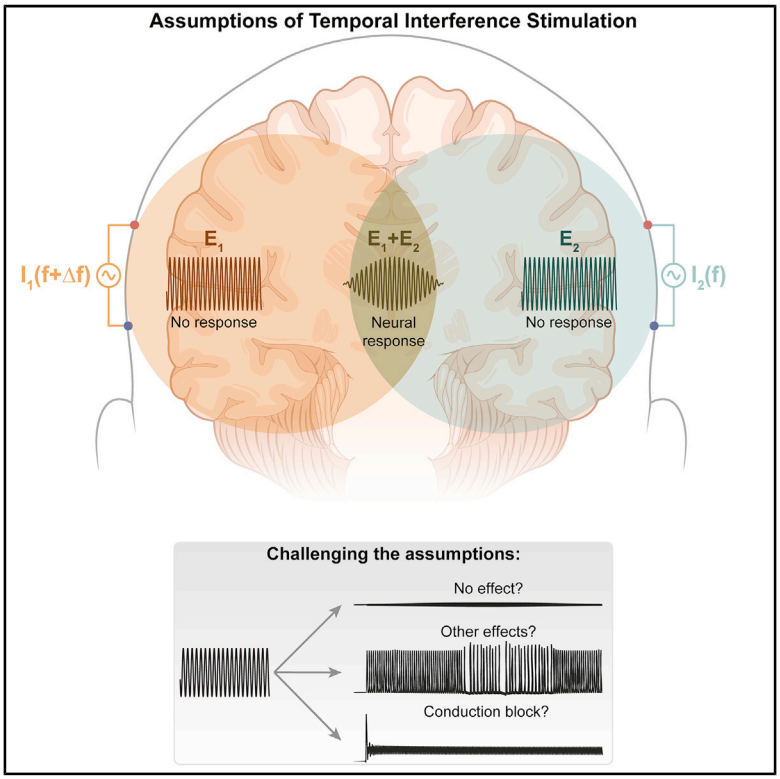

Authors

Ehsan Mirzakhalili, Beatrice Barra, Marco Capogrosso, Scott F. Lempka

Correspondence

mcapo@pitt.edu (M.C.), lempka@umich.edu (S.F.L.)

In Brief

Mirzakhalili et al., studied the physics of neurostimulation through temporal interference (TI). They showed that an ion-channel-mediated current rectification mechanism (rather than low-pass filtering) is necessary for target neurons to respond to TI. However, this mechanism also leads to other response patterns, such as conduction block, in off-target structures.

Highlights

- We investigated the physics of neurostimulation with TI
- Ion-channel-mediated rectification of currents allows neurons to respond to TI
- Current rectification induces tonic firing and conduction block in off-target axons
- We argue for control experiments testing for conduction block in simple geometries

Mirzakhalili et al., 2020, Cell Systems *11*, 557–572
December 16, 2020
https://doi.org/10.1016/j.cels.2020.10.004

CellPress

Cell Systems

CellPress
OPEN ACCESS

Article

Biophysics of Temporal Interference Stimulation

Ehsan Mirzakhalili,[1,2] Beatrice Barra,[3,4] Marco Capogrosso,[4,5,6,8,*] and Scott F. Lempka[1,2,7,8,9,*]
[1]Department of Biomedical Engineering, University of Michigan, Ann Arbor, MI 48109, USA
[2]Biointerfaces Institute, University of Michigan, Ann Arbor, MI 48109, USA
[3]Department of Neuroscience and Movement Science, University of Fribourg, Fribourg, Switzerland
[4]Rehab and Neural Engineering Labs, University of Pittsburgh, Pittsburgh, PA 15213, USA
[5]Department of Neurological Surgery, University of Pittsburgh, Pittsburgh, PA 15213, USA
[6]Department of Bioengineering, University of Pittsburgh, Pittsburgh, PA 15213, USA
[7]Department of Anesthesiology, University of Michigan, Ann Arbor, MI 48109, USA
[8]These authors contributed equally
[9]Lead Contact
*Correspondence: mcapo@pitt.edu (M.C.), lempka@umich.edu (S.F.L.)
https://doi.org/10.1016/j.cels.2020.10.004

SUMMARY

Temporal interference (TI) is a non-invasive neurostimulation technique that utilizes high-frequency external electric fields to stimulate deep neuronal structures without affecting superficial, off-target structures. TI represents a potential breakthrough for treating conditions, such as Parkinson's disease and chronic pain. However, early clinical work on TI stimulation was met with mixed outcomes challenging its fundamental mechanisms and applications. Here, we apply established physics to study the mechanisms of TI with the goal of optimizing it for clinical use. We argue that TI stimulation cannot work via passive membrane filtering, as previously hypothesized. Instead, TI stimulation requires an ion-channel mediated signal rectification process. Unfortunately, this mechanism is also responsible for high-frequency conduction block in off-target tissues, thus challenging clinical applications of TI. In consequence, we propose a set of experimental controls that should be performed in future experiments to refine our understanding and practice of TI stimulation. A record of this paper's transparent peer review process is included in the Supplemental Information.

INTRODUCTION

The ability to manipulate neural activity without performing highly invasive surgical procedures would represent a major breakthrough in medicine (Musk and Neuralink, 2019; Perry, 2020). This type of technology would enable neurostimulation of deep tissue structures, such as the subthalamic nucleus to treat symptoms of Parkinson's diseases or spinal dorsal columns to treat refractory pain (Lempka and Patil, 2018; Lozano et al., 2019), without requiring invasive surgery. This capability would dramatically reduce costs and complications. In fact, it may even improve clinical outcomes by enabling more selective stimulation. Unfortunately, the realization of this technology is precluded by the physical laws governing the penetration of electromagnetic radiation within biological tissues. The electric potentials generated by electric currents delivered outside the skin rapidly decay with distance from the sources (Faria et al., 2011; Plonsey and Barr, 2007; Rush and Driscoll, 1968). As neural excitability is directly proportional to the strength of the extracellular electric potential (McNeal, 1976), it has not been possible to use non-invasive electric stimulation to activate deep regions without activating superficial neurons.

However, a recent study proposed that the low-pass filtering property of the neural membrane may be leveraged to provide non-invasive stimulation of deep brain regions (Grossman et al., 2017). This intrinsic low-pass filtering causes the neural membrane to be more sensitive to low-frequency oscillating fields relative to high-frequency fields. Hence, it was proposed that two electrode pairs could noninvasively stimulate deep brain structures by delivering high-frequency currents with a small frequency offset. At a specific region in space, superposition of the high-frequency currents would create a low-frequency pattern of amplitude modulation (AM). Within this region, neurons would respond to this low-frequency modulation due to the low-pass filtering properties of the neural membrane. This approach was termed temporal interference (TI) (Grossman et al., 2017) and had been proposed decades earlier under different names, such as interferential current therapy and interferential stimulation (Agharezaee and Mahnam, 2015; Goats, 1990). Translating these pivotal studies into successful clinical therapies requires an understanding of how TI fields are modulated within the human body (Cao and Grover, 2020; Karimi et al., 2019; Rampersad et al., 2019). In consequence, there is an ongoing healthy debate examining the clinical utility of this technology when considering the challenge of inefficient current penetration in large structures, such as the human head (Cao and Grover, 2018; Howell and McIntyre, 2020; Rampersad et al., 2019).

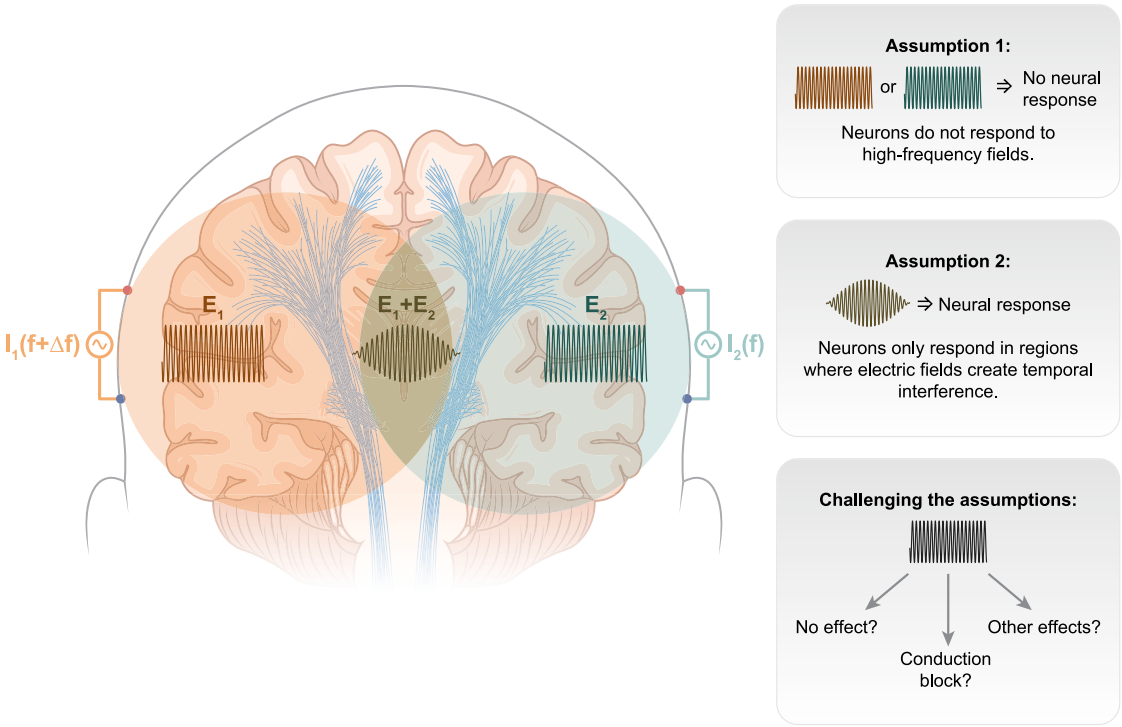

Figure 1. Concept of TI Stimulation

Two pairs of scalp electrodes (I_1 and I_2) apply high-frequency currents at a small frequency difference that generate oscillating electric fields within the brain ($\mathbf{E_1}$ and $\mathbf{E_2}$). At a certain region, superposition of these fields will lead to low-frequency AM ($\mathbf{E_1}$+$\mathbf{E_2}$). It is hypothesized that TI stimulation exclusively activates neurons in deep brain regions without affecting superficial areas. This approach assumes that superficial neurons will not respond to the high-frequency stimulation ($\mathbf{E_1}$ or $\mathbf{E_2}$) because of their intrinsic low-pass filtering properties (Assumption 1). Deep neurons will respond to TI stimulation because the interfering electrical fields contain low-frequency oscillating elements ($\mathbf{E_1}$+$\mathbf{E_2}$) (Assumption 2). However, research has demonstrated that neurons do respond to high-frequency electric fields (Challenging the assumptions).

As part of this debate, we aimed at addressing the fundamental physics underlying TI stimulation. In essence, the intriguing TI concept is based on two logically related assumptions (Figure 1):

(1) Neural membranes do not respond to high-frequency stimulation, or more precisely, they are more sensitive to slow oscillating fields, and in consequence:
(2) Neurons will only respond to TI stimulation within the spatial region where the electric field is modulated at the slower beat frequency (i.e., the small frequency offset between the two waveforms).

However, both of these assumptions are either oversimplifications or incorrect. Decades of research has shown that neural membranes do respond to high-frequency fields, albeit the dynamics become complex and lead to phenomena, such as conduction block (i.e., inhibition of action potential propagation) (Bhadra et al., 2007, 2019; Crosby et al., 2017; Joseph and Butera, 2009; Joseph et al., 2007; Kilgore and Bhadra, 2006; Tai et al., 2005; Zhang et al., 2006a, 2006b). This research has also shown that axons are more susceptible to polarization from (invasive and non-invasive) electric stimulation (Aberra et al., 2018; Chakraborty et al., 2018; Hause, 1975; Howell and McIntyre, 2020; McIntyre et al., 2004; Rahman et al., 2013; Ranck, 1975; Wongsarnpigoon and Grill, 2012). Specifically, action potentials can be initiated at the axon terminals, in correspondence to maxima of the electric field (Chakraborty et al., 2018; Hause, 1975; Hentall, 1985). In contrast, along the rest of the axon, action potential initiation sites correspond to peaks of the "activating function" (i.e., second-order spatial derivative of the electric potential along the axon) (Rattay, 1986). Therefore, excitation depends on multiple properties and orientation to the induced fields. Characterization of how these physical properties apply to TI stimulation is extremely important to understand and predict accurate neural activation profiles.

To address these important points, we used established physics to study TI within a simple theoretical framework. Our results support the experimental evidence that it is possible to excite distant neural structures in phase with the low-frequency envelope of the TI stimulus (Grossman et al., 2017). However, our results also show that the same mechanism enabling TI-driven excitation may also generate conduction block in off-target neural structures. These results highlight the need for precise control experiments in TI studies.

RESULTS

Fundamental Representation of the Physics of TI

Studying current propagation and neural activation with TI in complex geometries prevents the emergence of general

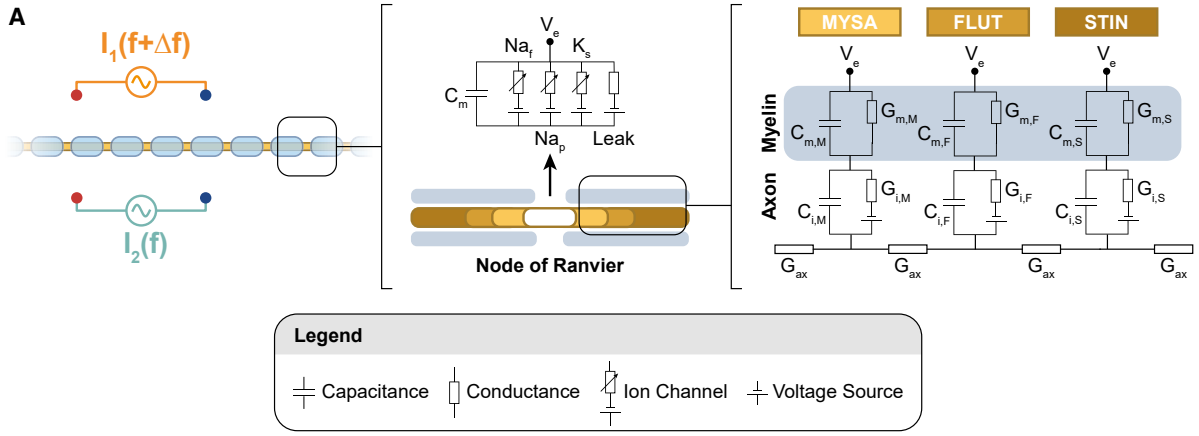

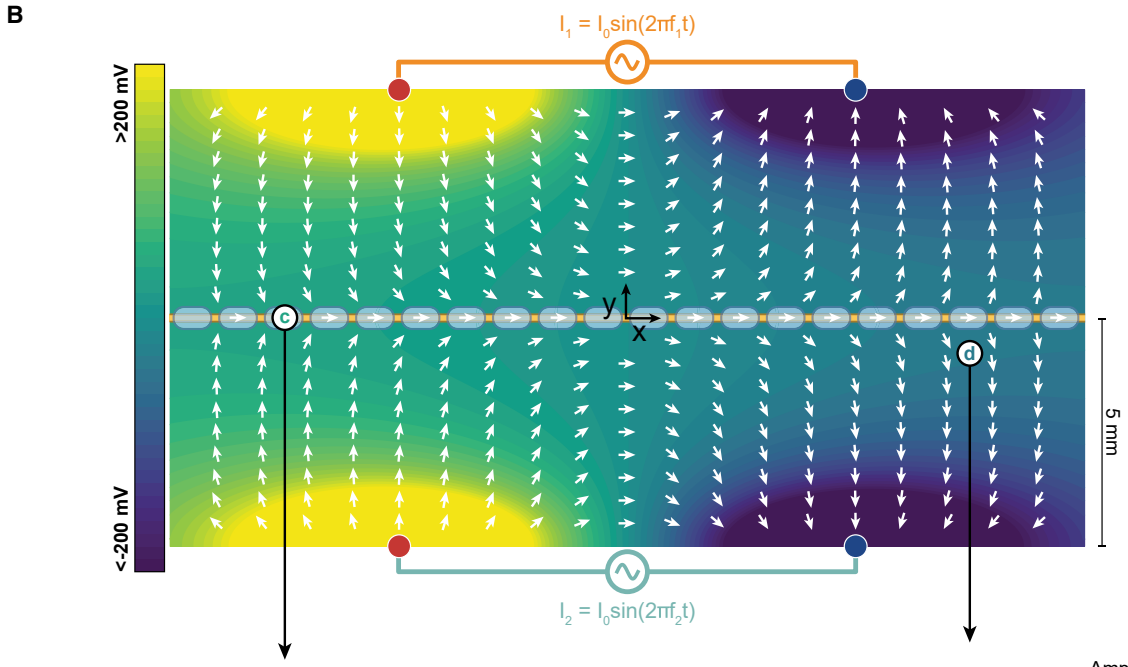

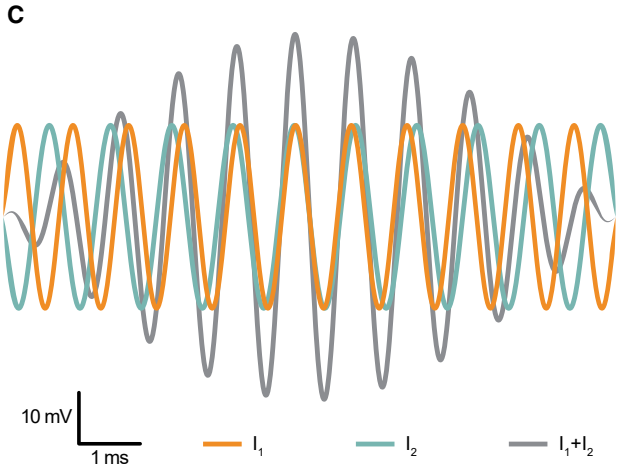

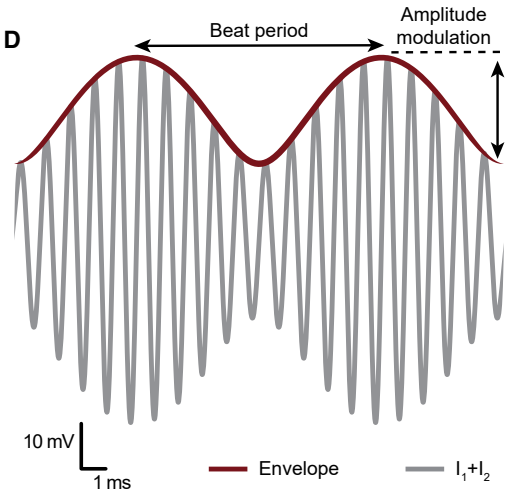

(legend on next page)

patterns, such as the sensitivity of neurons to field orientation. Furthermore, it requires numerical solutions of Maxwell's equations, which may further hamper prediction accuracy (Howell et al., 2014; Pelot et al., 2018). We reasoned that studying TI within a simple geometry would allow for straightforward characterization of electric field and neural excitability properties that could be generalized. Therefore, we considered a set of parallel axons in an infinite homogeneous space traversing temporally interfering fields generated by two pairs of current sources oriented parallel to the axons (Figure 2A). With this setup, we were able to utilize analytic solutions of Maxwell's equations and straightforward characterization of the neural membrane responses in relation to field orientation. This simple system can be viewed as a prototype of a clinical system for targeting white matter tracts deep within the brain, axons within a peripheral nerve, or longitudinal dorsal column axons in the spinal cord.

We represented electrodes as pairs of ideal point sources and analytically calculated the corresponding potentials under quasi-static conditions (Plonsey and Heppner, 1967) using the superposition principle. To mimic the electrical properties of nerve or white matter tissues, we considered the space as an anisotropic infinite volume, i.e., currents were more likely to spread along the direction of the axons (Capogrosso et al., 2013; Foster and Schwan, 1989; Ranck and BeMent, 1965). At the electrode pairs, we then applied sinusoidal currents of equal strength oscillating at high frequencies f_1 and f_2, where $f_1 - f_2 << f_1$ or f_2 (Figure 2B) (see STAR Methods).

Figure 2B shows the electric potential at an instant in time in which the strength of the total field at any point in space was at its maximum. As expected, the absolute value of the electric potential was larger near the current sources. Moreover, the potential field near each current source was only slightly affected by the other current sources. However, at the midline, where the distance from each opposing electrode is equal, the potential field was affected equally by each electrode pair. This location was where the constructive/destructive interference of fields from each electrode was most evident (Figure 2C). Analytically, in all points in space, the strength of the potential field (the envelope) oscillates between $|V_1 + V_2|$ and $|V_1 - V_2|$ at a frequency of $f_1 - f_2$ (beat frequency), where V_1 and V_2 are the peak spatial voltages generated by the first and second electrode pairs, respectively (Figure 2D—see STAR Methods).

To calculate the neural response to TI stimulation, we then applied these spatiotemporal voltages to a multicompartment axon model that utilized the standard Hodgkin-Huxley formalism (Figure 2A) and solved the time-dependent partial differential cable equations using the software package, NEURON (Hines and Carnevale, 1997) (see STAR Methods).

Neural Membranes Must Rectify the Electric Potential to Generate Extrinsic Neural Activity

At an equal distance between the electrode pairs, the TI voltage waveform showed a clear low-frequency envelope (Figures 2C and 3A). Development of TI was driven by the hypothesis that neurons could respond to this low-frequency oscillating envelope rather than to the high-frequency stimuli. However, being the sum of two sinusoidal fields, the TI stimulus waveform only contains high-frequency content ("TI stimulation" power spectrum in Figure 3A). Neural membranes are known to have passive, low-pass filtering properties because of the capacitive-resistive properties of the lipid bilayer membrane (Hutcheon and Yarom, 2000). However, a simple low-pass filter only reduces the power of the high-frequency components, as no low-frequency components are actually present in the stimulus ("low-pass filter" power spectrum in Figure 3B). Low-pass filtering alone cannot extract this envelope because the low-frequency and high-frequency oscillating components of the stimulus are multiplied by each other (see Equation 12 in the STAR Methods) and not summed (Oppenheim et al., 1968). Therefore, despite previous claims (Grossman et al., 2017), the low-pass filtering properties of neurons are unlikely to be the underlying mechanism for TI stimulation.

However, the envelope of the TI stimulus can be extracted if the stimulus is rectified and then low-pass filtered ("demodulator" power spectrum in Figure 3C). Rectifying a signal before low-pass filtering is an established method of demodulating multiplied and convolved signals (Oppenheim et al., 1968). In fact, prior experimental results have suggested that the cellular response to the envelope of high-frequency signals occurs through nonlinear processes, such as half-wave rectification (Middleton et al., 2006).

To examine if neural membranes perform rectification in response to TI stimulation, we applied a subthreshold TI stimulus to the axon. We observed high-frequency oscillations of the membrane voltage, but the moving average of the membrane voltage showed low-frequency oscillations ("full axon model" in Figure 3E). Moreover, the power spectrum of the membrane voltage contained frequency elements that were exactly equal to the beat frequency ("full axon model" power spectrum in Figure 3E). Therefore, the axon had properties that enable the demodulation of an amplitude-modulated stimulus. However, the axon did not perform as a perfect demodulator because

Figure 2. Fundamental Representation of the Physics of TI

(A) In our system, myelinated axons (not drawn to scale) are placed between two electrode pairs. Each electrode pair is placed 5 mm away from the axon and electrodes are 10 mm apart. The first and second electrode pair, I_1 and I_2, receive a zero-phase sinusoidal current with a frequency of f_1 and f_2, respectively. The axon compartment model includes explicit representation of myelinated regions comprised of the myelin attachment segment (MYSA), paranode main segment (FLUT), and internode segment (STIN) regions of the fiber and nodes of Ranvier. The nodes of Ranvier include fast and persistent sodium channels, slow potassium channels, and leakage current.

(B) Contours of the total potential field generated by the superposition of all four individual electrodes. The contours are plotted at z = 0, where z represents depth. The vectors represent the electric field in a logarithmic scale.

(C) The voltages generated by each electrode pair and their sum at point *c* (−7.5,0,0) mm. The small frequency difference between the electrode pairs results in TI of electric fields generated by each electrode pair.

(D) The net potential field and the envelope for its strength at point *d* (+7.5, −1,0) mm. The envelope oscillates with the "beat" frequency. AM is defined as the difference between the maximum and the minimum of the envelope. We used $I_0 = 1\ mA$, $f_1 = 1,100\ Hz$, $f_2 = 1,000\ Hz$, $\sigma_{xx} = 0.6\ S/m$, $\sigma_{yy} = \sigma_{zz} = 0.083\ S/m$ to generate the results in this figure. See STAR Methods for details.

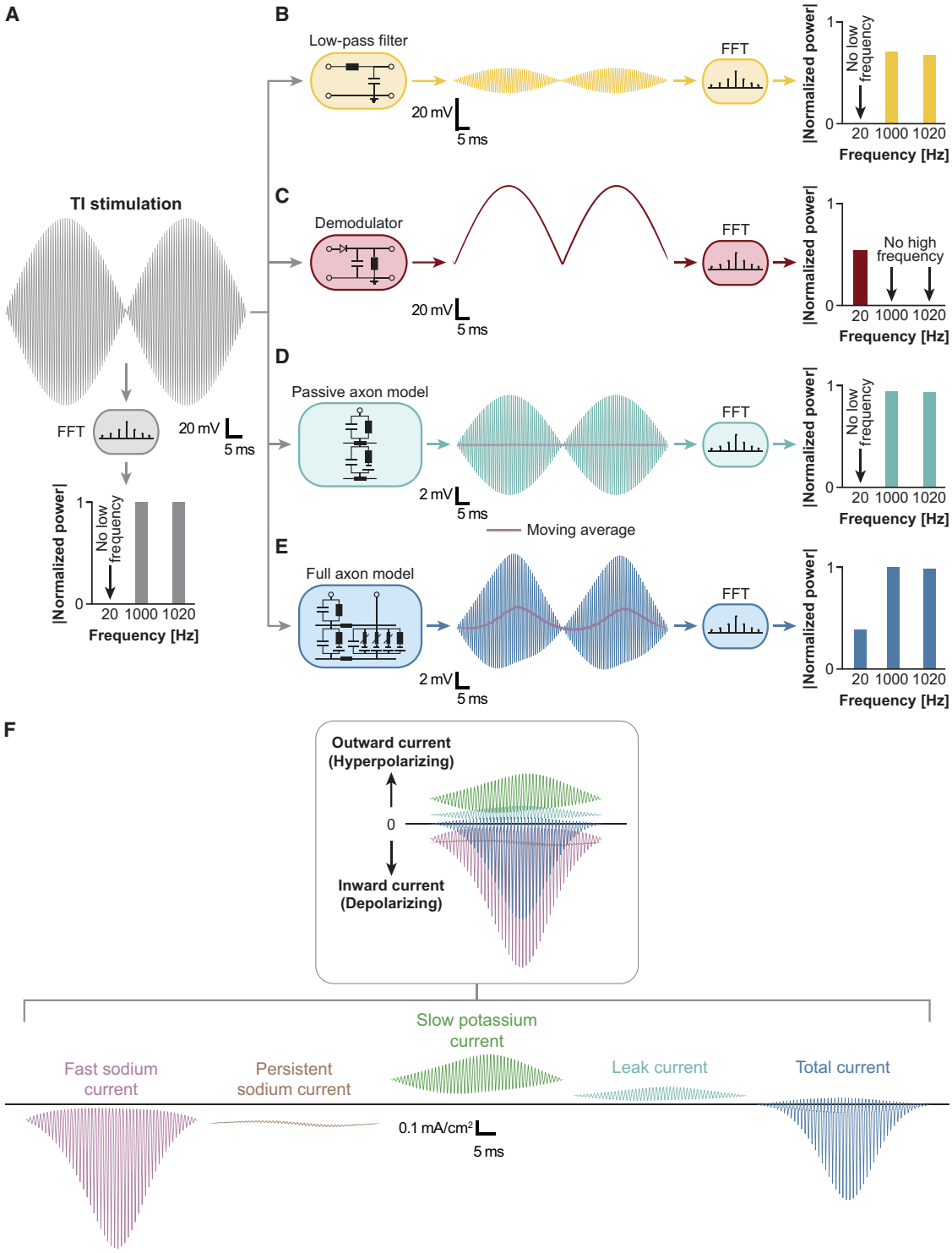

Figure 3. Neural Membranes must Rectify the Electric Potential to Generate Extrinsic Neural Activity

(A) Signal analysis of TI stimulation and subthreshold membrane oscillations. We used a carrier frequency of 1,000 Hz and a beat frequency of 20 Hz to generate TI stimulation. The power spectrum of the TI stimulation obtained by fast Fourier transform (FFT) shows that the TI stimulation waveform does not include any low-frequency content.

(B) Low-pass filtering of the TI stimulation only attenuates the stimulation and does not extract the low-frequency oscillations.

(C) However, a demodulator, which rectifies the signal before low-pass filtering it, extracts the low-frequency oscillations.

(legend continued on next page)

high-frequency oscillations were obvious in the membrane voltage and the frequency content still contained high-frequency elements.

We hypothesized that rectification arises from nonlinearities in the ion channel dynamics and that this rectification is necessary for demodulation of the TI stimulus. To test our hypothesis, we applied the same subthreshold TI stimulus to a passive axon in which we had removed all active ion channels. Again, the membrane voltage showed high-frequency oscillations, but we observed no rectification as the moving average was equal to the resting voltage ("passive axon model" in Figure 3D). Furthermore, the low-frequency content associated with the beat frequency was also absent in the power spectrum for the passive axon ("passive axon model" power spectrum in Figure 3D). Therefore, low-pass filtering properties of neurons are not sufficient to extract the envelope of the TI stimulation and rectification is necessary.

We hypothesized that this quasi-rectification must be generated by a preference of the active neuron membrane to inject or eject currents through ion channels. Therefore, we investigated each of the ion currents passing through the membrane during a subthreshold TI stimulus (Figure 3F). At a node of Ranvier close to the stimulating electrodes, the fast Na^+ current clearly dominated the other currents and generated a total inward current, which depolarized the axon. Hence, rectification occured at the membrane because the increase in Na^+ channel conductance was larger than the increase in K^+ channel conductance. This rectification also occurred because of the specific gating properties of fast Na^+ channels, in which they activate more rapidly than they inactivate in response to depolarization. We also observed that the rectification properties were closely related to the resonance behavior of the axon (Figure S1) and could predict the optimum TI frequency (the beat frequency that resulted in the lowest activation threshold). In consequence of these rectification properties, additional analysis showed that TI produces membrane excitation only when the envelope of the stimulation is near its maximum (Figure S2).

TI Excitation Is Governed by Amplitude Modulation of the Electric Field for Axon Terminals and the Activating Function for Long Axons

We then investigated the action potential initiation sites in response to TI stimulation, and more specifically, which field variables determine the location of these initiation sites (Figure 4A). This question is of high practical value since hypothetical medical devices using TI must be tuned to direct neural activation toward certain spatial targets within the brain or other regions of the nervous system. Understanding which field variables drive excitation would allow such therapeutic tuning.

Previous studies on TI suggested that the variable that predicts the area of activation was related to the electric field, and specifically, the region where temporal modulation of the electric field was maximal (Grossman et al., 2017). However, decades of research have shown that the electric field is not the only factor driving excitation in response to extracellular stimulation (Ladenbauer et al., 2010; McNeal, 1976; Rattay, 1986, 1990). Indeed, the electrophysiological properties of neurons and axons can be represented as networks of resistors and capacitors using a method developed in the 19th century by Lord Kelvin, known as cable theory (Thomson, 1856). In cable theory, the corresponding second-order partial differential equation describes the electrical behavior of an axon. By examining this equation, it is clear that the initial response along an axon membrane to an external electrical stimulus is driven by the second-order spatial derivative of the extracellular voltages along the axon. This term is well known as the "activating function" (Rattay, 1986). Instead, at axon terminals embedded in external electrical fields, the initial response is determined by the electric field.

Following this reasoning, we believed that the neural response to TI stimulation would obey similar principles as traditional stimulation paradigms. Hence, we hypothesized that TI excitation would be related to the electric field for stimulation near an axon terminal while it would be related to the activating function for stimulation along the remaining axon. Therefore, we investigated the location of action potential initiation along the axon in response to TI stimulation (Figure 4). We performed analyses for stimulation both near the end and middle of the axon. We compared different field variables to the location of action potential initiation and looked if the maxima of these variables matched the action potential initiation sites. We considered the following quantities: AM of the electric potential, electric field (as previously proposed [Grossman et al., 2017]), and the activating function (second-order derivative of the electric potential). For this analysis, we used carrier frequencies of 1, 2, and 4 kHz, and tested beat frequencies of 1–50 Hz in steps of 1 Hz (see STAR Methods and Supplemental Information). We determined the activation sites for all of the beat and carrier frequencies. We pooled data to provide a distribution of activation sites and a description of initiation sites for TI stimulation in general instead of initiation sites for specific carrier and beat frequencies.

For stimulation applied near the axon terminals, we compared the spatial behavior of each field variable to the position of the action potential initiation sites. Figures 4B–4D summarize these calculations and clearly show that action potentials are most likely to be generated where AM of the electric field is maximal. We also observed that the carrier and beat frequency contents were both maximum at the nodes of Ranvier where AM of the electric field is maximum (see Figure S1D). This finding supports previous speculations that AM of the electric field is the driving force for TI stimulation (Grossman et al., 2017).

In contrast, for stimulation along longitudinal axons, we observed some interesting differences. First, we observed that axons did not possess only one but two dominant action potential initiation sites (histograms in Figures 4E–4G). Second, when comparing the spatial behavior of each field variable to the position of these initiation sites, Figure 4F clearly shows that action potentials were most likely to be generated where AM of the activating function is maximal. Furthermore, we observed that the

(D) A passive (no active ion channels) axon performs similarly to a low-pass filter and is not affected by the beat frequency of the TI stimulation.
(E) However, the subthreshold membrane oscillations of the axon with voltage-gated ion channels show low-frequency content in its power spectrum.
(F) Asymmetry in ion currents enable the axon to rectify the stimulation. At a node of Ranvier close to the stimulating electrodes, there is a net inward current that produces the membrane depolarization shown in (E).

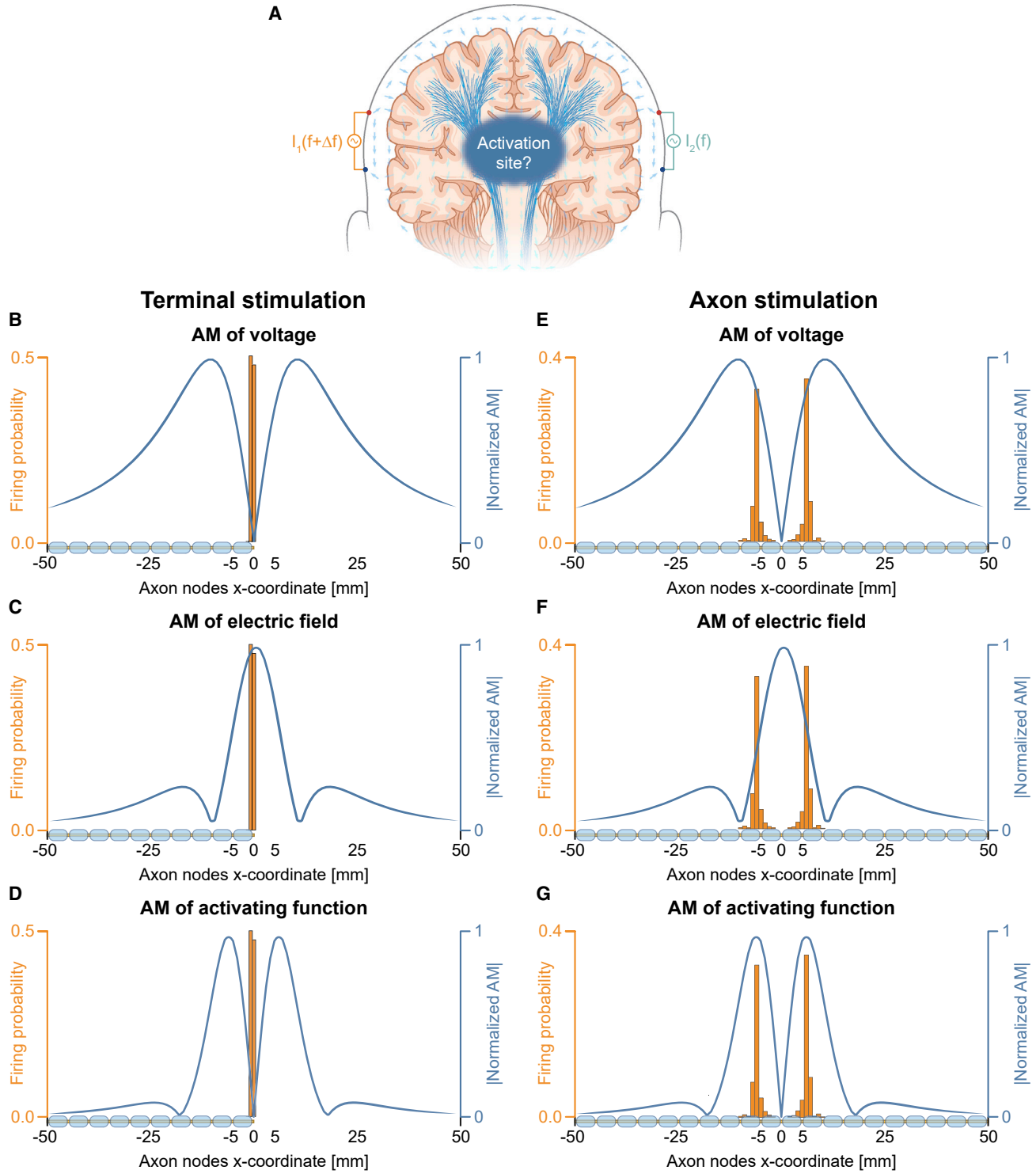

Figure 4. TI Excitation Is Governed by AM of the Electric Field or the Activating Function

(A) To optimize TI technologies, it is critical to understand where in space axons generate action potentials in response to TI stimulation and which field variables determine the location of these initiation sites.

(B) For TI stimulation near the axon terminal (node 100 at x = 0 mm), the action potential sites do not match the peaks of normalized AM of the electric potential.

(C) However, the action potential sites match the peaks of normalized AM of the electric field in the direction of the axon.

(D) No action potentials are generated where normalized AM of the activating function is maximum.

(legend continued on next page)

carrier frequency content and the beat frequency content were both maximum at the nodes of Ranvier where AM of the activating function is maximum (see Figure S1G). These findings contradict previous speculations that AM of the electric field is the sole driving force for TI stimulation (Grossman et al., 2017). In fact, no action potentials are initiated where AM of the electric field is maximum (Figure 4F). These results support the concept that AM of the activating function along axons is the driving force for neural activity generated by TI stimulation. This result is analogous to the activating function concept shown in traditional neurostimulation applications (McNeal, 1976; Rattay, 1986).

Multiple Classes of Neural Responses Are Observed during TI Stimulation

Previous studies have suggested that the neural response to TI stimulation is binary, i.e., neurons are either activated in phase with the stimulus envelope or they remain silent. This scenario was based on experimental data suggesting that neurons located near the maximum AM were activated, while neurons in the same region did not respond to the high-frequency stimulation generated by an individual pair of electrodes (Grossman et al., 2017). However, several works have shown that neurons do respond to high-frequency signals similar to those applied by individual electrode pairs in TI stimulation. However, the neural response to the kilohertz-frequency stimulation is quite complex and exhibits several classes of operating domains or effect states (Bhadra et al., 2019). For example, neurons can have only an initial response to the stimulation or they can fire continuously throughout the duration of the stimulus (Crosby et al., 2017; Lempka et al., 2015; Zander et al., 2020). Another phenomenon observed during the kilohertz-frequency stimulation is known as the "conduction block" (Bhadra et al., 2019). During conduction block, the kilohertz-frequency stimulus blocks or inhibits action potential propagation along an axon. High-frequency conduction block has been extensively studied because of its potential indications for neuroprosthetic technologies. Given the complexity of neural responses observed in previous studies of kilohertz-frequency stimulation, we hypothesized that axons may also exhibit multiple operating domains during TI stimulation.

We then extended our previous results to all regions of space and examined these domains throughout our system (Figure 5). We tuned stimulation amplitude using the activation threshold for the optimum beat frequency of 5 Hz (see Figure S1) and a carrier frequency of 2 kHz (Figure 5B). To compare the effects of TI and No-TI ($f_1 = f_2$) stimulation, we also used the same minimum activation threshold and stimulated axons with a control stimulation protocol where the beat frequency was zero between the current pairs (Figure 5C).

As expected from our previous results, we observed phasic neural activity for axons at the midline (y = 0 mm) during TI stimulation. However, the No-TI stimulation showed only initial onset activity (Figure 5C). Therefore, TI stimulation seems to elicit activity in the deeper tissue when the No-TI stimulation fails to do so. Axons located farther away from the midline and closer to one individual pair of electrodes experienced smaller AM but overall higher-amplitude stimuli (e.g., y = 1.7 and 3.5 mm in Figure 5A) and these axons were not expected to respond to the low-frequency modulating envelope. Indeed, at y = 1.7 mm from the midline, we observed tonic neural activity for both TI and No-TI stimulation (Figures 5B and 5C). This result indicates that tonic neural firing may occur at the border of the region of maximal AM. Finally, moving even closer to the electrode pairs (e.g. y = 3.5 mm), we observed a region where only onset activity occurred for both TI and No-TI stimulation (Figures 5B and 5C). Axons were otherwise silent for the duration of the stimuli. The presence of such a region supports the idea that regions of low AM cannot be activated with high-frequency stimuli alone.

However, we wanted to verify that axons that appeared silent were not actually in a state of conduction block. Conduction block is typically observed as an initial period of onset activity followed by a quiescent period in which no action potentials can propagate past the stimulus focus (Bhadra et al., 2019). To test for conduction block, we followed the common methodology of injecting a test pulse at one end of the axon (node 0) and examining if the resultant action potential successfully propagated to the other end of the axon (node 100) (Figure 5D) (Bhadra et al., 2007; Lempka et al., 2015). If the resultant action potential failed to propagate to the other end of the axon, then the axon was in a state of conduction block that inhibited action potential propagation. Figure 5D shows the results of the conduction block test. For the No-TI stimulation and the axon at y=0 mm, we clearly observed that the test pulse traveled through the axon, which indicated a quiescence axon. However, at y = 3.5 mm, the test pulse did not travel through the axon, which indicated that conduction block had occurred. We observed conduction block for both TI and No-TI stimuli. Thus, the absence of activity in the regions of low or no AM can be due to conduction block. The results described above and shown in Figure 5 are for stimulation applied near the middle of the axon (node 50 at x = 0 mm). We performed the same analysis for stimulation applied near the end of the axon (node 100 at x = 0 mm) and we observed similar trends for both TI and No-TI stimulation (Figures S3–S5).

The "Sandwich" Hypothesis

Accurately characterizing the spatial distribution of these response types is critical to understand if TI can effectively stimulate deep neural structures, especially if this excitation comes at the cost of blocking neural activity in more superficial tissues. Therefore, to further characterize the response types generated during TI stimulation, we examined the firing patterns of all axons located between the electrodes in increments of 0.1 mm (Figure 6). We performed this analysis for both TI and No-TI controls applied near the middle of the axon. We summarized the raster

(E) For TI stimulation near the middle of the axon (node 50 at x = 0 mm), the action potential sites do not match the peaks of normalized AM of the electric potential.
(F) The action potential sites also do not match the peaks of normalized AM of the electric field in the direction of the axon.
(G) However, the action potential sites match the peaks of normalized AM of the activating function in the direction of the axon.
The histograms in (B–D) and (E–G) show the probability of action potential initiation at each node of Ranvier in the axon model for TI stimulation near the axon terminal and axon middle, respectively. The histograms were obtained from the collective results for beat frequencies of 1–50 Hz and carrier frequencies of 1, 2, and 4 kHz. Note, the axons shown on the x axis are not drawn to scale.

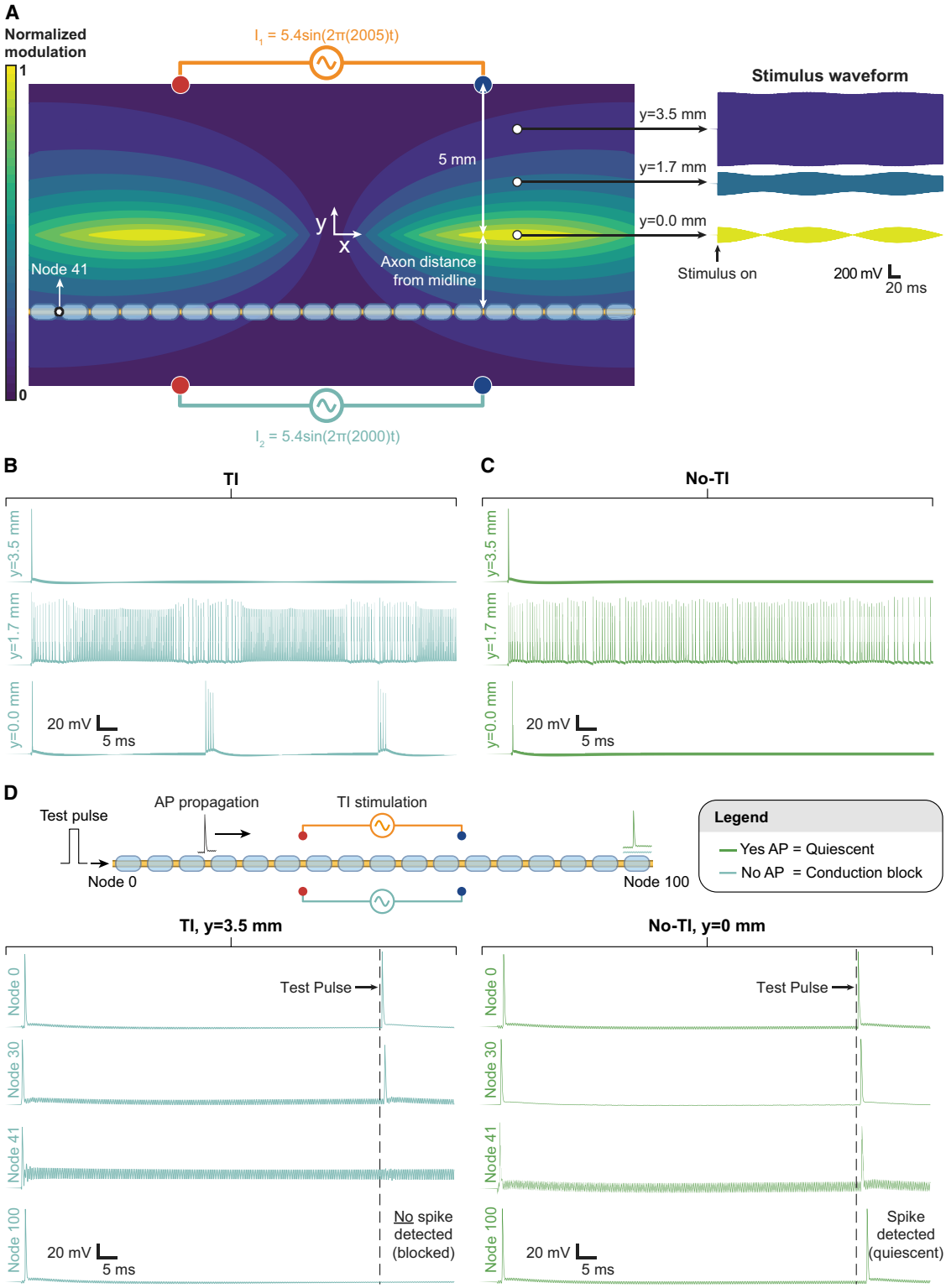

Figure 5. Multiple Classes of Neural Responses Are Observed during TI Stimulation

(A) The contours show AM of the activating function in the x-direction along the direction of the axons. The contours are plotted at z = 0, where z represents depth. AM of the activating function is maximum at the midline. The right column shows the extracellular voltages generated by the TI stimulus at different locations. The stimulus strength is larger closer to individual electrodes while its AM is smaller. We examined the TI response of axons located at y = 0 mm (midline), y = 1.7 mm, and y = 3.5 mm.

(legend continued on next page)

plots as firing rates. The bar plots represent the steady-state firing behavior of the axons as a function of distance from the midline. Based on the summary of the raster plots, we classified axon firing rates into the following response classes: quiescent, blocked, phasic, or tonic. For TI stimulation, we observed a phasic regime near the center while these axons were quiescent for the No-TI stimulation (Figures 6A and 6B). Therefore, TI stimulation activated axons in a deep region, whereas the No-TI stimulation failed to activate the same axons.

However, as we moved away from the midline, we also observed regions of phasic activity followed by regions of tonic activity for both TI and No-TI stimulations. The presence of these two regions shows that a strong stimulus with little-to-no AM can also activate axons at the margin of the TI-effective spatial region. Next, we observed a region of conduction block for both TI and No-TI stimulations. Moving closer to the electrodes resulted in another small region of tonic activity for the TI and No-TI stimulations. Finally, we observed the outmost superficial layers to be blocked for both TI and No-TI stimulations. We termed this spatial pattern a "sandwich," as layers of tonic firing and conduction block alternated and covered the deep TI-responsive region.

As our results contradicted the initial hypothesis motivating the development of TI as a non-invasive neuromodulation strategy, we wanted to verify that our mathematical modeling was robust to parameter variation and not a result of specific parameters. Therefore, we performed a parameter sensitivity analysis by varying the time constants of the ion channels in our axon model (see STAR Methods). We changed the forward and backward rates of the channel states equally so that the time constants were altered by ±25% while the steady-state activation profiles remained unchanged. Note that we needed to adjust the activation thresholds when we changed the model parameters (see STAR Methods). Figures 6C and 6D show that our results are consistent across 50% variation in the parameter range (and even across a larger parameter range, see Figure S4). We performed the same analysis for all of the carrier frequencies (1, 2, and 4 kHz) and beat frequencies (2, 5, and 20 Hz) that we considered in this study (Figure S3) and for stimulation applied near the end of the axon (Figures S3A and S4A). Even though the size of the specific regions changed, the relative sandwich pattern remained largely unchanged and showed that these results are robust. Notably, we did not observe conduction block when utilizing a carrier frequency of 1 kHz (Figure S3) or after a 50% decrease in the time constant of the fast sodium channel activation variable (τ_m) (Figure S4). Under these conditions, the carrier frequencies were below the minimum block frequency; however, we still observed multiple response classes (quiescent, phasic, and tonic) (see Supplemental Information). These results suggest that the neural response to TI is not binary. Stimulation parameters necessary to produce TI activation at deep regions also likely produce multiple response types, including tonic firing and conduction block, in more superficial neural tissue at both axon terminals and along axons.

As large-diameter axons have the lowest threshold to extracellular stimulation (McNeal, 1976), we performed our simulations with model axons with a fiber diameter of 8.7 μm that can be found within peripheral nerves, the spinal cord, and the corticospinal tract (Feirabend et al., 2002; Terao et al., 1994; Ugrenović et al., 2016). However, the brain has an abundance of small-diameter axons (Benavides-Piccione et al., 2020). Therefore, we also tested our "sandwich" hypothesis for a range of fiber diameters by performing the same analysis shown in Figure 6. We found that the general "sandwich" response did not change for small or large fibers (Figure S5), except for 2.0-μm diameter fibers for which we did not observe conduction block. Small 2.0-μm diameter fibers exhibited phasic activation near the midline and tonic firing in more superficial fibers (Figure S5). For 2.0-μm diameter fibers, conduction block could be possible at higher frequencies (e.g. 5–20 kHz) than the carrier frequencies considered in our study (Pelot et al., 2017). The lack of conduction block may also indicate a limitation of our axon model at small diameters because it has not been validated in this range (Pelot et al., 2017). However, even for small fiber diameters, it was not possible to generate a TI response in deep axons without producing undesired effects, such as tonic firing or conduction block, in more superficial axons. It is also important to note that the activation thresholds for small-diameter fibers were much higher than the activation thresholds for large axons. For example, the activation threshold (carrier frequency of 2 kHz, beat frequency of 5 Hz, and stimulation near the middle of the fiber) for a fiber at the midline with a diameter of 8.7 μm was 5.4 mA, while the activation threshold for a fiber with a diameter of 2.0 μm was 108.5 mA. Therefore, targeting small-diameter fibers within the brain or elsewhere in the nervous system will most likely activate and/or induce conduction block in large-diameter fibers before modulating activity in the target small-diameter fibers.

(B) Axonal activity during TI stimulation at node 0 (first node of Ranvier) for axons located at y = 0.0 mm (midline), y = 1.7 mm, and y = 3.5 mm. The stimulation current for all simulations was 5.4 mA, which was the activation threshold for the axon located at the midline during TI stimulation for a carrier frequency of 2 kHz and the optimum beat frequency of 5 Hz. The axon at y = 3.5 mm shows only onset activity. The axon at y = 1.7 mm shows tonic activity. The axon at y = 0.0 mm shows phasic activity with periods equal to the beat frequency of the stimulus.

(C) Axonal activity during No-TI stimulation at node 0 (first node of Ranvier) for axons located at y = 0.0 mm (midline), y = 1.7 mm, and y = 3.5 mm. The stimulation current for all simulations was 5.4 mA, which was the activation threshold for the axon located at the midline during TI stimulation. Both electrode pairs received 2-kHz current ($f_1 = f_2$), which resulted in no AM. The axons at y=0.0 mm and y=3.5 mm only show an onset response. The axon at y=1.7-mm shows tonic activity similar to TI stimulation.

(D) Conduction block test. To test for potential conduction block in axons, we injected a test pulse strong enough to initiate an action potential (AP) at node 0 and checked if the action potential propagated to the other end of the axon at node 100. If an AP was detected, the axon was quiescent. Otherwise, conduction block had occurred. We tested if the nature of onset activity for axons under TI and No-TI at y = 3.5 mm was different from the axon under No-TI at y = 0.0 mm. The left column shows the conduction block test for the axon at y = 3.5 mm during TI stimulation. The test AP does not reach the other end of the axon. Hence, conduction block has occurred (we obtained the same result for No-TI, data not shown). The right column shows the conduction block test for the axon at y = 0 mm during No-TI stimulation. The test pulse reaches the other end of the axon. Hence, the axon is quiescent and conduction block has not occurred.

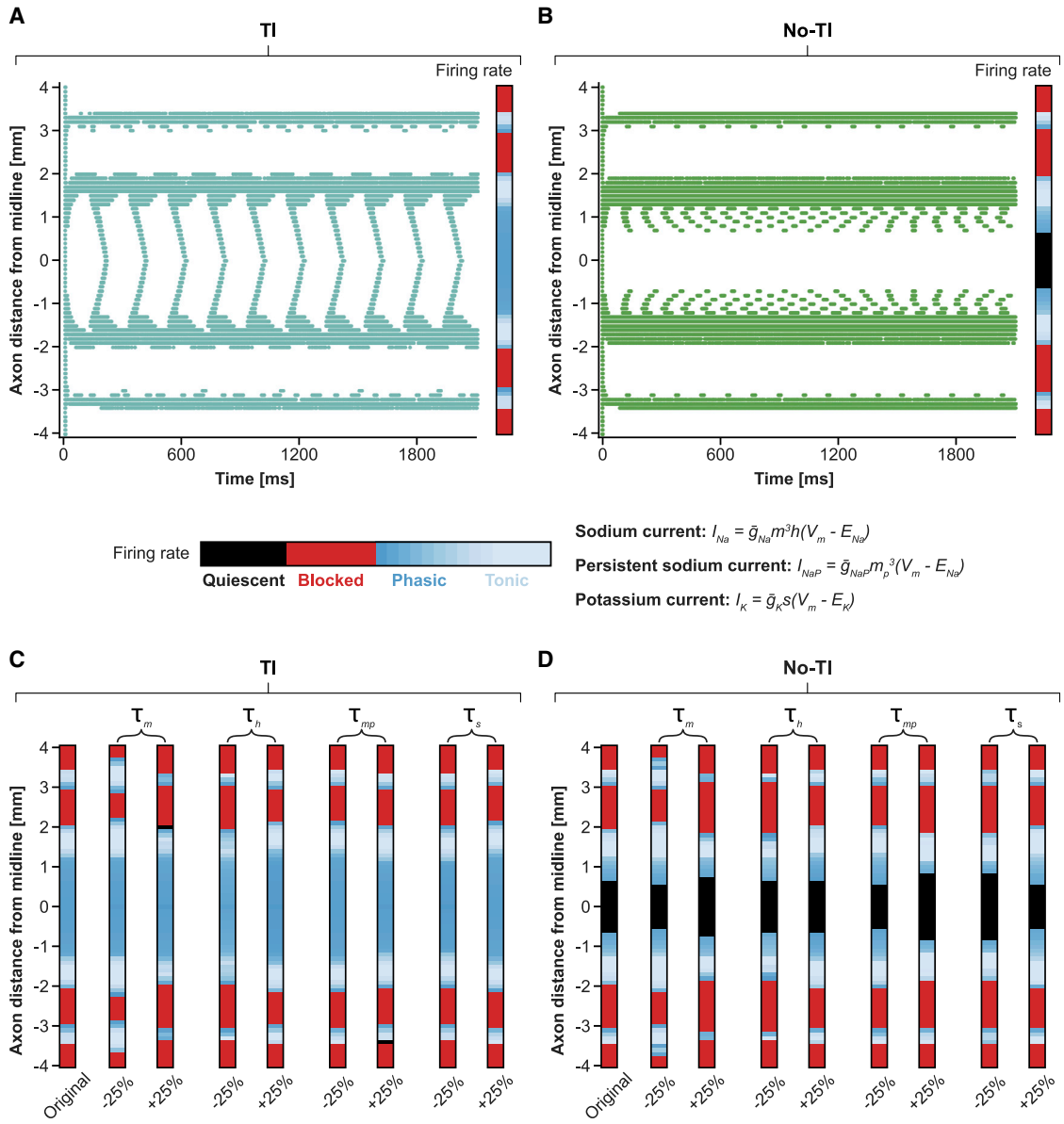

Figure 6. The "Sandwich" Hypothesis

(A) Axonal activity regimes for TI stimulation. We studied the response of axons that were placed from −4.0 to +4.0 mm away from the midline in increments of 0.1 mm and stimulation applied near the middle of the axon (node 50 at x = 0 mm). The stimulation current was equal to the activation threshold for the axon located at the midline for a carrier frequency of 2,000 Hz and the optimum beat frequency of 5 Hz. The raster plots indicate APs detected at node 0. We performed the conduction block test for axons that only exhibited onset activity. We summarized the raster plots as firing rates. The raster plots are mostly symmetric with only small differences near the electrodes as the axon experiences two different frequencies (2,000 Hz near the bottom and 2,005 Hz near the top) closer to the electrode pairs. The midline region shows phasic activity followed by a band of tonic activity. There are two conduction block regions near the electrode pairs. There is also a small band of tonic activity between the blocked regimes.

(B) Axonal activity regimes for No-TI stimulation. The raster plots are symmetric because both electrode pairs received 2-kHz current. The No-TI activity regimes follow the same composition as the TI stimulation except at the midline (region of maximum AM), where the No-TI response is quiescent while TI stimulation shows phasic activity.

(C and D) The layered axonal response regimes are valid for a large parameter space. We changed the forward and backward rates of each ion channel type to increase or decrease gating variable time constants by ±25%. While the size of the specific regions changes, the relative pattern remains unchanged and shows that these results are robust. Note that we needed to adjust the activation threshold when we changed the parameters of the model (see STAR Methods).

DISCUSSION

In this study, we presented simple physical calculations to systematically characterize the neural responses to TI stimulation. Our results provide theoretical support for the neural responses to TI observed in single-cell *in vitro* experiments (Grossman et al., 2017). However, our results demonstrate that the previously proposed mechanism of passive membrane filtering is insufficient

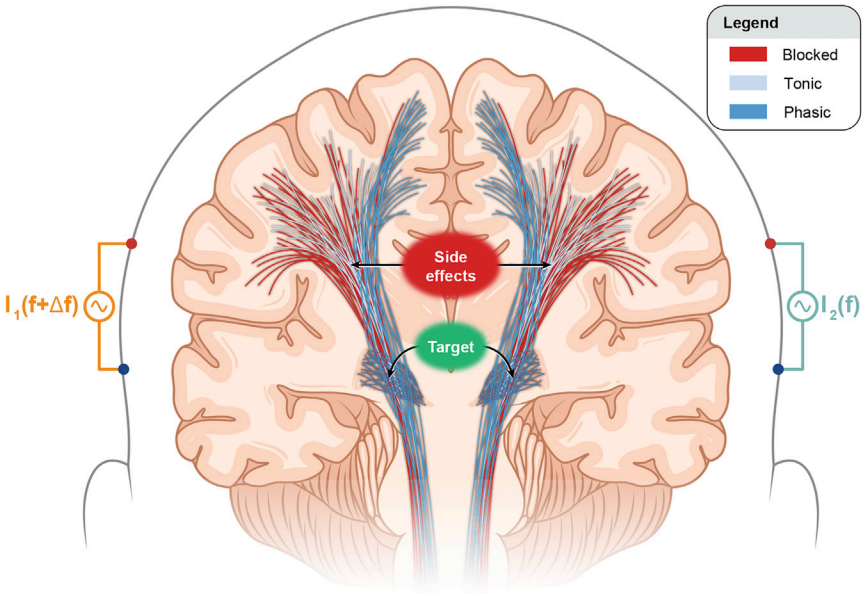

Figure 7. Clinical Implications of TI Stimulation

TI stimulation can produce multiple types of neural responses. TI stimulation may provide therapeutic benefit by inducing the desired phasic responses in the target neural populations (e.g., subthalamo-pallidal pathway—"Target" axons—to relieve motor symptoms associated with Parkinson's disease). However, this phasic excitation may come at the cost of producing additional responses (e.g., tonic firing and conduction block) in untargeted areas (e.g., corticospinal tract—"Side effects" axons) that may produce undesired side effects. This issue is critical to the development of efficacious clinical therapies that utilize TI stimulation.

for TI excitation because the TI stimulus does not contain any low-frequency information. Instead, an active ion-channel mediated signal rectification process is required for TI excitation. Unfortunately, this mechanism is also linked to the phenomenon of high-frequency conduction block, which has significant implications for the application of TI for clinical neurostimulation therapies.

Indeed, in our study, it was not possible to produce TI responses without also inducing activation and/or conduction block in non-targeted areas that could generate unwanted side effects. We summarized these response patterns with the "sandwich" hypothesis, which contradicts the previous interpretation of experimental results on TI. At the current amplitudes required to generate sufficiently strong AM in the deep tissue, more superficial layers will be subjected to higher-amplitude non-modulated fields that will force neurons in these regions to respond with tonic firing or conduction block. This is a simple and obvious consequence of the inverse distance relationship of electromagnetic radiation within a conductive medium that is independent of geometry. In fact, this consequence will likely be exacerbated by the distance between electrodes and target tissues at the scale of the human head (Howell and McIntyre, 2020). Therefore, we believe that the "sandwich" hypothesis must be considered in the tentative design of TI neuromodulation technologies.

For example, one attractive application of TI technologies would be non-invasive deep brain stimulation to treat a variety of neurological and psychiatric conditions, such as Parkinson's disease (Grossman et al., 2018; Lozano et al., 2019). Current deep brain stimulation approaches to treat Parkinson's disease involve implantation of electrodes in deep brain areas, such as the subthalamic nucleus. One putative mechanism of deep brain stimulation of the subthalamic nucleus is the activation of the subthalamo-pallidal pathway ("Target" axons in Figure 7) to alleviate the motor symptoms of Parkinson's disease (Johnson et al., 2008). However, the therapeutic range of deep brain stimulation is limited by unwanted side effects (e.g., contralateral muscle contractions) that are generated when stimulation spreads outside of the target and activates other pathways that pass nearby the subthalamic nucleus (e.g., the corticospinal tract—"Side effects" axons in Figure 7). Therefore, deep brain stimulation technologies must have sufficient selectivity to activate the target areas to produce the desired symptom relief while avoiding modulation of non-target areas that produce undesired side effects. This required selectivity may represent a major challenge for TI technologies because our results suggest that the parameters necessary to generate phasic activation in the target pathways (e.g., the subthalamo-pallidal pathway) would likely produce phasic activation, tonic activation, and/or conduction block in superficial pathways (e.g., the corticospinal pathway) that would cause undesired side effects (Figure 7).

Our theoretical analysis is based on established and simple physical calculations. This approach allowed us to make conclusions that can be experimentally tested. Specifically, our study demands for controls assessing potential conduction block and other response patterns generated in experimental studies of TI. In light of our results, experimental studies that only control for TI-like responses during TI versus No-TI in the target region do not constitute a correct experimental design. We found that neurons in the deep regions fire in phase with the envelope of the TI stimulus while being silent during standard high-frequency stimulation. Therefore, investigation of the behavior of non-targeted layers becomes critical to proving the efficacy of TI stimulation. Grossman et al., performed experiments in the mouse brain examining changes in *c-fos* expression as a marker of neural activity (Grossman et al., 2017). These experiments showed that while TI stimulation elicited an increase in *c-fos* expression in the hippocampus, it did not produce significant changes in *c-fos* expression in superficial cortical (non-targeted) regions. This result suggests that for the specific regions investigated, TI stimulation elicited a response in the deep tissue and not in the superficial layers. However, it is important to recognize that because *c-fos* protein is mostly induced in nuclei of neurons (Dragunow and Robertson, 1987), *c-fos* expression can only be an indicator of somatic activity (Gao and Ji, 2009). Therefore, the general validity of this method is limited because: (1) at high firing rates, antidromic action potentials may fail to successfully

propagate into the somata of certain classes of neurons due to large discrepancies in conduction properties between the axon and the large somas (Anderson et al., 2018; Yi and Grill, 2018) and impedance mismatch (Fuortes et al., 1957; Goldstein and Rall, 1974); (2) axons may be recruited in some areas and blocked in others, thus preventing antidromic activity from reaching the somata; and (3) non-expression of *c-fos* is not an indicator of conduction block. These combined insights highlight the limitation of experimental controls that do not directly test for conduction block but rather for positive neural activation. Perhaps, experiments on simpler geometries, such as peripheral nerves, may help in the design of these controls.

Grossman et al., proposed TI as a potential non-invasive alternative to DBS (i.e., suprathreshold stimulation) (Grossman et al., 2017). Therefore, in this study, we investigated conditions necessary for the direct recruitment of axons, which are most susceptible to polarization (Aberra et al., 2018; Chakraborty et al., 2018; Howell and McIntyre, 2020; McIntyre et al., 2004; Rahman et al., 2013; Wongsarnpigoon and Grill, 2012). However, there is significant theoretical and experimental evidence that non-invasive transcranial electrical stimulation approaches do not generate the electric fields necessary to produce direct excitation (Datta et al., 2009; Rampersad et al., 2019; Vöröslakos et al., 2018). A recent computational modeling study investigated a large number of parameter sets to optimize the penetration depths of TI stimulation, including the pallidum, which is directly relevant to the example presented in Figure 7 (Rampersad et al., 2019). For a stimulation current of 2 mA (a common value used in human experiments) (Lefaucheur et al., 2017), the maximum electric field anywhere in the brain and in any direction was <0.8 V/m. This electric field was well below the range necessary to activate deep brain or cortical structures with conventional stimulation (~28–120 V/m) (Åström et al., 2015; Radman et al., 2009; Rampersad et al., 2019) and the range necessary for TI stimulation in our study (10–30 and 38–107 V/m near the end and middle of the axon, respectively). Therefore, TI would require much higher current values than normally used in non-invasive stimulation and likely induce the block effects we observed in our theoretical analysis.

However, multiple studies have also highlighted the possibility of transcutaneous stimulation, including TI, to provide subthreshold neuromodulation rather than direct activation of neurons. In this case, electric fields and currents are used to bias synaptic transmission by polarizing axon terminals (Chakraborty et al., 2018; Rahman et al., 2013). Polarization effects that alter neural firing, synaptic transmission, and subthreshold currents can be obtained with lower field strengths compared with direct recruitment (~1 V/m) (Berényi et al., 2012; Datta et al., 2009; Fröhlich and McCormick, 2010; Ozen et al., 2010; Vöröslakos et al., 2018). It may be possible to obtain these subthreshold fields strengths with TI stimulation and to direct TI fields toward specific deep brain regions by utilizing specific electrode montages, electrode sizes, and multiple waveforms (Cao and Grover, 2020; Howell and McIntyre, 2020; Huang and Parra, 2019; Rampersad et al., 2019). It may also be possible to exploit cellular or network features that are specific to certain brain regions (Esmaeilpour et al., 2019) to maximize the subthreshold effects of TI stimulation. Moreover, the potential effects of transcutaneous stimulation, including TI, may not be limited to neurons. For example, it has been suggested that glial cells may be affected by transcranial electric stimulation (Gellner et al., 2016; Mishima et al., 2019; Ruohonen and Karhu, 2012). Some of these phenomena have been preliminarily explored by Grossman et al., in their safety assessment of TI with no evidence of anatomical side effects (Grossman et al., 2017). Nevertheless, future TI studies should consider these effects and perhaps other possible neuromodulatory effects of non-invasive stimulation, such as modulation of synaptic plasticity (Ranieri et al., 2012) or cerebral blood flow (Wachter et al., 2011). In our study, we focused on direct neural activation with TI stimulation and did not explore these subthreshold properties or effects on glial cells. Therefore, future work should be directed toward these areas to complement our results and reach a general understanding of TI as a potential neuromodulation technology.

In summary, we believe that the results of this study will help ensure that future work can begin on a solid theoretical understanding of the neural response to TI stimulation. If TI is to evolve into a mature and clinically effective technology, these theoretical concepts must be considered in the design of clinical technologies.

STAR★METHODS

Detailed methods are provided in the online version of this paper and include the following:

- KEY RESOURCES TABLE
- RESOURCE AVAILABILITY
  - Lead Contact
  - Materials Availability
  - Data and Code Availability
- METHOD DETAILS
  - Temporal Interference (TI) Stimulation
  - Point Source Voltage Distribution
  - Amplitude Modulation (AM) and Beat Frequency
  - Myelinated Axon Model
  - Morphology
  - Ionic Currents
  - Model Implementation

SUPPLEMENTAL INFORMATION

Supplemental Information can be found online at https://doi.org/10.1016/j.cels.2020.10.004.

ACKNOWLEDGMENTS

We would like to thank Dr. Esra Neufeld and Dr. Antonino Cassara from the IT IS foundation in Zurich for the useful and enriching discussions on temporal interference. We are grateful to Dr. Cameron McIntyre (Case Western Reserve University) for his valuable critique of our study. We would also like to thank Dr. Lee Fisher (University of Pittsburgh) for having listened to our endless discussions about the science in this manuscript during the North American Neuromodulation Society meeting in Las Vegas, NV. We would also like to thank the reviewers for helping to significantly improve the quality of this manuscript. Finally, from the supervisors, we thank Ehsan and Beatrice for having worked on this manuscript even during the stressful times of the COVID-19 pandemic.

AUTHOR CONTRIBUTIONS

Conceptualization, E.M., B.B., M.C., and S.F.L.; Methodology, E.M., B.B., M.C., and S.F.L.; Software, E.M.; Formal Analysis, E.M.; Data Curation,

E.M.; Writing – Original Draft, E.M., B.B., M.C., and S.F.L.; Writing – Reviewing & Editing, E.M., B.B., M.C., and S.F.L.; Visualization, E.M., B.B., M.C., and S.F.L.; Supervision, M.C. and S.F.L.; Project Administration, M.C. and S.F.L.; Funding Acquisition, M.C. and S.F.L.

DECLARATION OF INTERESTS

S.F.L. has equity in Hologram Consultants, LLC and is a member of the scientific advisory board for Abbott Neuromodulation. S.F.L. holds stock options, received research support, and serves on the scientific advisory board of Presidio Medical. M.C. is the inventor of several patents involving technologies for the electrical stimulation of the spinal cord. All other authors declare no competing interests.

Received: June 19, 2020
Revised: August 21, 2020
Accepted: October 6, 2020
Published: November 5, 2020

REFERENCES

Aberra, A.S., Peterchev, A.V., and Grill, W.M. (2018). Biophysically realistic neuron models for simulation of cortical stimulation. J. Neural Eng. *15*, 066023.

Agharezaee, M., and Mahnam, A. (2015). A computational study to evaluate the activation pattern of nerve fibers in response to interferential currents stimulation. Med. Biol. Eng. Comput. *53*, 713–720.

Anderson, R.W., Farokhniaee, A.A., Gunalan, K., Howell, B., and McIntyre, C.C. (2018). Action potential initiation, propagation, and cortical invasion in the hyperdirect pathway during subthalamic deep brain stimulation. Brain Stimul. *11*, 1140–1150.

Åström, M., Diczfalusy, E., Martens, H., and Wårdell, K. (2015). Relationship between neural activation and electric field distribution during deep brain stimulation. IEEE Trans. Biomed. Eng. *62*, 664–672.

Benavides-Piccione, R., Regalado-Reyes, M., Fernaud-Espinosa, I., Kastanauskaite, A., Tapia-González, S., León-Espinosa, G., Rojo, C., Insausti, R., Segev, I., and DeFelipe, J. (2020). Differential structure of hippocampal CA1 pyramidal neurons in the human and mouse. Cereb. Cortex *30*, 730–752.

Berényi, A., Belluscio, M., Mao, D., and Buzsáki, G. (2012). Closed-loop control of epilepsy by transcranial electrical stimulation. Science *337*, 735–737.

Bhadra, N., Lahowetz, E.A., Foldes, S.T., and Kilgore, K.L. (2007). Simulation of high-frequency sinusoidal electrical block of mammalian myelinated axons. J. Comput. Neurosci. *22*, 313–326.

Bhadra, N., Vrabec, T., Kilgore, K., and Bhadra, N. (2019). Activation of the sciatic nerve evoked during epidural spinal cord stimulation in rodents. Bioelectron. Med. *2*, 63–71.

Bossetti, C.A., Birdno, M.J., and Grill, W.M. (2008). Analysis of the quasi-static approximation for calculating potentials generated by neural stimulation. J. Neural Eng. *5*, 44–53.

Cao, J., and Grover, P. (2018). Do single neuron models exhibit temporal interference stimulation? In 2018 IEEE Biomedical Circuits and Systems Conference (BioCAS), pp. 1–4.

Cao, J., and Grover, P. (2020). STIMULUS: noninvasive dynamic patterns of neurostimulation using spatio-temporal interference. IEEE Trans. Biomed. Eng. *67*, 726–737.

Capogrosso, M., Wenger, N., Raspopovic, S., Musienko, P., Beauparlant, J., Bassi Luciani, L.B., Courtine, G., and Micera, S. (2013). A computational model for epidural electrical stimulation of spinal sensorimotor circuits. J. Neurosci. *33*, 19326–19340.

Chakraborty, D., Truong, D.Q., Bikson, M., and Kaphzan, H. (2018). Neuromodulation of axon terminals. Cereb. Cortex *28*, 2786–2794.

Crosby, N.D., Janik, J.J., and Grill, W.M. (2017). Modulation of activity and conduction in single dorsal column axons by kilohertz-frequency spinal cord stimulation. J. Neurophysiol. *117*, 136–147.

Datta, A., Bansal, V., Diaz, J., Patel, J., Reato, D., and Bikson, M. (2009). Gyri-precise head model of transcranial direct current stimulation: improved spatial focality using a ring electrode versus conventional rectangular pad. Brain Stimul. *2*, 201–207, 207.e1.

Dragunow, M., and Robertson, H.A. (1987). Kindling stimulation induces c-fos protein(s) in granule cells of the rat dentate gyrus. Nature *329*, 441–442.

Dwyer, J., Lee, H., Martell, A., and van Drongelen, W. (2012). Resonance in neocortical neurons and networks. Eur. J. Neurosci. *36*, 3698–3708.

Esmaeilpour, Z., Kronberg, G., Parra, L.C., and Bikson, M. (2019). Temporal interference stimulation targets deep brain regions by modulating neural oscillations. bioRxiv. https://doi.org/10.1101/2019.12.25.888412.

Faria, P., Hallett, M., and Miranda, P.C. (2011). A finite element analysis of the effect of electrode area and inter-electrode distance on the spatial distribution of the current density in tDCS. J. Neural Eng. *8*, 066017.

Feirabend, H.K.P., Choufoer, H., Ploeger, S., Holsheimer, J., and Van Gool, J.D. (2002). Morphometry of human superficial dorsal and dorsolateral column fibres: significance to spinal cord stimulation. Brain *125*, 1137–1149.

Foster, K.R., and Schwan, H.P. (1989). Dielectric properties of tissues and biological materials: a critical review. Crit. Rev. Biomed. Eng. *17*, 25–104.

Fröhlich, F., and McCormick, D.A. (2010). Endogenous electric fields may guide neocortical network activity. Neuron *67*, 129–143.

Fuortes, M.G.F., Frank, K., and Becker, M.C. (1957). Steps in the production of motoneuron spikes. J. Gen. Physiol. *40*, 735–752.

Gao, Y.J., and Ji, R.R. (2009). c-Fos and pERK, which is a better Marker for neuronal activation and central sensitization after noxious stimulation and tissue tnjury? Open Pain J. *2*, 11–17.

Gellner, A.K., Reis, J., and Fritsch, B. (2016). Glia: a neglected player in non-invasive direct current brain stimulation. Front. Cell. Neurosci. *10*, 188.

Goats, G.C. (1990). Interferential current therapy. Br. J. Sports Med. *24*, 87–92.

Goldstein, S.S., and Rall, W. (1974). Changes of action potential shape and velocity for changing core conductor geometry. Biophys. J. *14*, 731–757.

Grossman, N., Bono, D., Dedic, N., Kodandaramaiah, S.B., Rudenko, A., Suk, H.J., Cassara, A.M., Neufeld, E., Kuster, N., Tsai, L.-H., et al. (2017). Noninvasive deep brain stimulation via temporally interfering electric fields. Cell *169*, 1029–1041.e16.

Grossman, N., Okun, M.S., and Boyden, E.S. (2018). Translating temporal interference brain stimulation to treat neurological and psychiatric conditions. JAMA Neurol *75*, 1307–1308.

Hause, L. (1975). A mathematical model for transmembrane potentials secondary to extracellular fields. Electroanesth Biomed. Biophys. Stud. 176–200.

Hentall, I.D. (1985). The membrane potential along an ideal axon in a radial electric field. Brain Res. *336*, 387–389.

Higgs, M.H., and Spain, W.J. (2009). Conditional bursting enhances resonant firing in neocortical layer 2–3 pyramidal neurons. J. Neurosci. *29*, 1285–1299.

Hille, B. (2001). Ion Channels of Excitable Membranes (Sinauer Associates, Inc.).

Hines, M.L., and Carnevale, N.T. (1997). The NEURON simulation environment. Neural Comput. *9*, 1179–1209.

Hines, M.L., Davison, A.P., and Muller, E. (2009). NEURON and python. Front. Neuroinform. *3*, 1.

Howell, B., and McIntyre, C.C. (2020). Feasibility of interferential and pulsed transcranial electrical stimulation for neuromodulation at the human scale. Neuromodulation. https://doi.org/10.1111/ner.13137.

Howell, B., Naik, S., and Grill, W.M. (2014). Influences of interpolation error, electrode geometry, and the electrode-tissue interface on models of electric fields produced by deep brain stimulation. IEEE Trans. Biomed. Eng. *61*, 297–307.

Hu, H., Vervaeke, K., Graham, L.J., and Storm, J.F. (2009). Complementary theta resonance filtering by two spatially segregated mechanisms in CA1 hippocampal pyramidal neurons. J. Neurosci. *29*, 14472–14483.

Huang, Y., and Parra, L.C. (2019). Can transcranial electric stimulation with multiple electrodes reach deep targets? Brain Stimul *12*, 30–40.

Hutcheon, B., and Yarom, Y. (2000). Resonance, oscillation and the intrinsic frequency preferences of neurons. Trends Neurosci *23*, 216–222.

Johnson, M.D., Miocinovic, S., McIntyre, C.C., and Vitek, J.L. (2008). Mechanisms and targets of deep brain stimulation in movement disorders. Neurotherapeutics *5*, 294–308.

Joseph, L., and Butera, R.J. (2009). Unmyelinated Aplysia nerves exhibit a nonmonotonic blocking response to high-frequency stimulation. IEEE Trans. Neural Syst. Rehabil. Eng. *17*, 537–544.

Joseph, L., Haeffele, B.D., and Butera, R.J. (2007). Conduction block induced by high frequency AC stimulation in unmyelinated nerves. In 29th Annual International Conference of the IEEE Engineering in Medicine and Biology Society (IEEE), pp. 1719–1722.

Karimi, F., Attarpour, A., Amirfattahi, R., and Nezhad, A.Z. (2019). Computational analysis of non-invasive deep brain stimulation based on interfering electric fields. Phys. Med. Biol. *64*, 235010.

Kilgore, K.L., and Bhadra, N. (2006). High frequency mammalian nerve conduction block: simulations and experiments. In International Conference of the IEEE Engineering in Medicine and Biology Society (IEEE), pp. 4971–4974.

Ladenbauer, J., Minassian, K., Hofstoetter, U.S., Dimitrijevic, M.R., and Rattay, F. (2010). Stimulation of the human lumbar spinal cord with implanted and surface electrodes: A computer simulation study. IEEE Trans. Neural Syst. Rehabil. Eng. *18*, 637–645.

Lefaucheur, J.P., Antal, A., Ayache, S.S., Benninger, D.H., Brunelin, J., Cogiamanian, F., Cotelli, M., De Ridder, D., Ferrucci, R., Langguth, B., et al. (2017). Evidence-based guidelines on the therapeutic use of transcranial direct current stimulation (tDCS). Clin. Neurophysiol. *128*, 56–92.

Lempka, S.F., McIntyre, C.C., Kilgore, K.L., and Machado, A.G. (2015). Computational analysis of kilohertz frequency spinal cord stimulation for chronic pain management. Anesthesiology *122*, 1362–1376.

Lempka, S.F., and Patil, P.G. (2018). Innovations in spinal cord stimulation for pain. Curr. Opin. Biomed. Eng. *8*, 51–60.

Lozano, A.M., Lipsman, N., Bergman, H., Brown, P., Chabardes, S., Chang, J.W., Matthews, K., McIntyre, C.C., Schlaepfer, T.E., Schulder, M., et al. (2019). Deep brain stimulation: current challenges and future directions. Nat. Rev. Neurol. *15*, 148–160.

McIntyre, C.C., Grill, W.M., Sherman, D.L., and Thakor, N.V. (2004). Cellular effects of deep brain stimulation: model-based analysis of activation and inhibition. J. Neurophysiol. *91*, 1457–1469.

McIntyre, C.C., Richardson, A.G., and Grill, W.M. (2002). Modeling the excitability of mammalian nerve fibers: influence of afterpotentials on the recovery cycle. J. Neurophysiol. *87*, 995–1006.

McNeal, D.R. (1976). Analysis of a model for excitation of myelinated. IEEE Trans. Biomed. Eng. BME- *23*, 329–337.

Middleton, J.W., Longtin, A., Benda, J., and Maler, L. (2006). The cellular basis for parallel neural transmission of a high-frequency stimulus and its low-frequency envelope. Proc. Natl. Acad. Sci. USA *103*, 14596–14601.

Mishima, T., Nagai, T., Yahagi, K., Akther, S., Oe, Y., Monai, H., Kohsaka, S., and Hirase, H. (2019). Transcranial direct current stimulation (tDCS) induces adrenergic receptor-dependent microglial morphological changes in mice. eNeuro *6*, 0204–19.2019.

Musk, E.; Neuralink (2019). An integrated brain-machine interface platform with thousands of channels. J. Med. Internet Res. *21*, e16194.

Narayanan, R., and Johnston, D. (2007). Long-term potentiation in rat hippocampal neurons is accompanied by spatially widespread changes in intrinsic oscillatory dynamics and excitability. Neuron *56*, 1061–1075.

Oppenheim, A.V., Schafer, R.W., and Stockham, T.G. (1968). Nonlinear filtering of multiplied and convolved signals. Proc. IEEE *56*, 1264–1291.

Ozen, S., Sirota, A., Belluscio, M.A., Anastassiou, C.A., Stark, E., Koch, C., and Buzsáki, G. (2010). Transcranial electric stimulation entrains cortical neuronal populations in rats. J. Neurosci. *30*, 11476–11485.

Pelot, N.A., Behrend, C.E., and Grill, W.M. (2017). Modeling the response of small myelinated axons in a compound nerve to kilohertz frequency signals. J. Neural Eng. *14*, 046022.

Pelot, N.A., Thio, B.J., and Grill, W.M. (2018). Modeling current sources for neural stimulation in COMSOL. Front. Comput. Neurosci. *12*, 40.

Perry, T.S. (2020). Here's how Facebook's brain-computer interface development is progressing, IEEE Spectrum https://spectrum.ieee.org/view-from-the-valley/consumer-electronics/portable-devices/heres-how-facebooks-braincomputer-interface-development-is-progressing.

Peters, M.J., and Elias, P.J.H. (1988). On the magnetic field and the electrical potential generated by bioelectric sources in an anisotropic volume conductor. Med. Biol. Eng. Comput. *26*, 617–623.

Plonsey, R., and Barr, R.C. (2007). Bioelectricity (Springer).

Plonsey, R., and Heppner, D.B. (1967). Considerations of quasi-stationarity in electrophysiological systems. Bull. Math. Biophys. *29*, 657–664.

Radman, T., Ramos, R.L., Brumberg, J.C., and Bikson, M. (2009). Role of cortical cell type and morphology in subthreshold and suprathreshold uniform electric field stimulation in vitro. Brain Stimul *2*, 215–228, 228.e1.

Rahman, A., Reato, D., Arlotti, M., Gasca, F., Datta, A., Parra, L.C., and Bikson, M. (2013). Cellular effects of acute direct current stimulation: somatic and synaptic terminal effects. J. Physiol. *591*, 2563–2578.

Rampersad, S., Roig-Solvas, B., Yarossi, M., Kulkarni, P.P., Santarnecchi, E., Dorval, A.D., and Brooks, D.H. (2019). Prospects for transcranial temporal interference stimulation in humans: a computational study. Neuroimage *202*, 116124.

Ranck, J.B. (1975). Which elements are excited in electrical stimulation of mammalian central nervous system: a review. Brain Res. *98*, 417–440.

Ranck, J.B., and BeMent, S.L. (1965). The specific impedance of the dorsal columns of cat: an inisotropic medium. Exp. Neurol. *11*, 451–463.

Ranieri, F., Podda, M.V., Riccardi, E., Frisullo, G., Dileone, M., Profice, P., Pilato, F., di Lazzaro, V., and Grassi, C. (2012). Modulation of LTP at rat hippocampal CA3-CA1 synapses by direct current stimulation. J. Neurophysiol. *107*, 1868–1880.

Rattay, F. (1990). Electrical Nerve Stimulation (Springer).

Rattay, F. (1986). Analysis of models for external stimulation of Axons. IEEE Trans. Biomed. Eng. BME- *33*, 974–977.

Rubinstein, J.T. (1993). Axon termination conditions for electrical stimulation. IEEE Trans Biomed. Eng. *40*, 654–663.

Ruohonen, J., and Karhu, J. (2012). TDCS possibly stimulates glial cells. Clin. Neurophysiol. *123*, 2006–2009.

Rush, S., and Driscoll, D.A. (1968). Current distribution in the brain from surface electrodes. Anesth. Analg. *47*, 717–723.

Tai, C., De Groat, W.C., and Roppolo, J.R. (2005). Simulation analysis of conduction block in unmyelinated axons induced by high-frequency biphasic electrical currents. IEEE Trans Biomed. Eng. *52*, 1323–1332.

Terao, S.i., Sobue, G., Hashizume, Y., Shimada, N., and Mitsuma, T. (1994). Age-related changes of the myelinated fibers in the human corticospinal tract: a quantitative analysis. Acta Neuropathol. *88*, 137–142.

Thomson, W. (1856). III. On the theory of the electric telegraph. Proc. R. Soc. Lond. A *7*, 382–399.

Tranchina, D., and Nicholson, C. (1986). A model for the polarization of neurons by extrinsically applied electric fields. Biophys. J. *50*, 1139–1156.

Ugrenović, S., Jovanović, I., Vasović, L., Kundalić, B., Čukuranović, R., and Stefanović, V. (2016). Morphometric analysis of the diameter and g-ratio of the myelinated nerve fibers of the human sciatic nerve during the aging process. Anat. Sci. Int. *91*, 238–245.

Vöröslakos, M., Takeuchi, Y., Brinyiczki, K., Zombori, T., Oliva, A., Fernández-Ruiz, A., Kozák, G., Kincses, Z.T., Iványi, B., Buzsáki, G., and Berényi, A. (2018). Direct effects of transcranial electric stimulation on brain circuits in rats and humans. Nat. Commun. *9*, 483.

Wachter, D., Wrede, A., Schulz-Schaeffer, W., Taghizadeh-Waghefi, A., Nitsche, M.A., Kutschenko, A., Rohde, V., and Liebetanz, D. (2011).

Transcranial direct current stimulation induces polarity-specific changes of cortical blood perfusion in the rat. Exp. Neurol. *227*, 322–327.

Wongsarnpigoon, A., and Grill, W.M. (2012). Computer-based model of epidural motor cortex stimulation: effects of electrode position and geometry on activation of cortical neurons. Clin. Neurophysiol. *123*, 160–172.

Yi, G., and Grill, W.M. (2018). Frequency-dependent antidromic activation in thalamocortical relay neurons: effects of synaptic inputs. J. Neural Eng. *15*, 056001.

Zander, H.J., Graham, R.D., Anaya, C.J., and Lempka, S.F. (2020). Anatomical and technical factors affecting the neural response to epidural spinal cord stimulation. J. Neural Eng. *17*, 036019.

Zhang, X., Roppolo, J.R., De Groat, W.C., and Tai, C. (2006a). Mechanism of nerve conduction block induced by high-frequency biphasic electrical currents. IEEE Trans. Biomed. Eng. *53*, 2445–2454.

Zhang, X., Roppolo, J.R., De Groat, W.C., and Tai, C. (2006b). Simulation analysis of conduction block in myelinated axons induced by high-frequency biphasic rectangular pulses. IEEE Trans. Biomed. Eng. *53*, 1433–1436.

STAR★METHODS

KEY RESOURCES TABLE

REAGENT or RESOURCE	SOURCE	IDENTIFIER
Software and Algorithms		
NEURON 7.7		https://www.neuron.yale.edu/neuron/
Python 3.7.3	Anaconda, Inc.	https://anaconda.org/
Simulation and analysis code	This paper	https://github.com/mirzakhalili/Mirzakhalili-et-al–CellSystems-2020

RESOURCE AVAILABILITY

Lead Contact

Further information and requests for resources should be directed to and will be fulfilled by the Lead Contact, Scott Lempka (lempka@umich.edu).

Materials Availability

This study did not generate new unique materials.

Data and Code Availability

- The source data in the paper can be produced by the computational code available at https://github.com/mirzakhalili/Mirzakhalili-et-al–CellSystems-2020
- The original code is available at https://github.com/mirzakhalili/Mirzakhalili-et-al–CellSystems-2020
- The scripts used to generate figures reported in this paper are available at https://github.com/mirzakhalili/Mirzakhalili-et-al–CellSystems-2020
- Any additional information required to reproduce this work is available from the Lead Contact.

METHOD DETAILS

Temporal Interference (TI) Stimulation

To model the extracellular voltage distributions generated during TI stimulation, we considered two pairs of electrodes. For the first electrode pair (electrodes located at [-5,+5,0] mm and [+5,+5,0] mm), we applied a sinusoidal current with the frequency, f_1. For the second electrode pair (electrodes located at [-5,-5,0] mm and [+5,-5,0] mm), we applied a sinusoidal current with the frequency, f_2. To calculate the overall potential field under quasistatic conditions (Bossetti et al., 2008; Plonsey and Heppner, 1967), we summed the individual potential fields generated by each electrode pair:

$$V_{total}(x,y,z,t) = V_1(x,y,z)\sin(2\pi f_1 t) + V_2(x,y,z)\sin(2\pi f_2 t) \quad \text{(Equation 1)}$$

where V_1 and V_2 are the potential fields generated by the first and second electrode pairs, respectively.

Point Source Voltage Distribution

We modeled electrodes as ideal point current sources. Under quasistatic conditions (Bossetti et al., 2008; Plonsey and Heppner, 1967), the total current ($\boldsymbol{J}$) in Maxwell's equations can be written as the sum of the source current ($\boldsymbol{J_s}$) and the conduction current ($\boldsymbol{\sigma \cdot E}$), where $\boldsymbol{\sigma}$ is the conductivity tensor and $\boldsymbol{E}$ is the electric field:

$$\boldsymbol{J} = \boldsymbol{J_s} + \boldsymbol{\sigma \cdot E} \quad \text{(Equation 2)}$$

Next, we applied the continuity condition to the current to obtain:

$$\nabla \cdot \boldsymbol{J} = \nabla \cdot \boldsymbol{J_s} + \nabla \cdot (\boldsymbol{\sigma} \cdot \boldsymbol{E}) = 0 \quad \text{(Equation 3)}$$

The electric field is related to the electric potential (V) field by:

$$\boldsymbol{E} = -\nabla V \quad \text{(Equation 4)}$$

Combining Equations 3 and 4, we obtained:

$$\nabla \cdot (\boldsymbol{\sigma} \cdot \nabla V) = \nabla \cdot \boldsymbol{J_s} \quad \text{(Equation 5)}$$

To mimic the electrical properties of nerve tissue, we placed the electrodes within an anisotropic infinite volume with a diagonal conductivity tensor. Assuming the conductivity tensor to be diagonal, we expanded Equation 5 in Cartesian coordinates as:

$$\sigma_{xx}\frac{\partial^2}{\partial x^2}V+\sigma_{yy}\frac{\partial^2}{\partial y^2}V+\sigma_{zz}\frac{\partial^2}{\partial z^2}V=\frac{\partial}{\partial x}(J_s)_x+\frac{\partial}{\partial y}(J_s)_y+\frac{\partial}{\partial z}(J_s)_z \quad \text{(Equation 6)}$$

where σ_{xx}, σ_{yy}, and σ_{zz} are the conductance in the x, y, and z directions, respectively. To solve Equation 6, we used the following non-dimensionalization procedure (Peters and Elias, 1988):

$$x^*=x\frac{\sqrt{\sigma_{yy}\sigma_{zz}}}{\sigma_0},y^*=y\frac{\sqrt{\sigma_{xx}\sigma_{zz}}}{\sigma_0},z^*=z\frac{\sqrt{\sigma_{xx}\sigma_{yy}}}{\sigma_0} \quad \text{(Equation 7)}$$

$$\left(J_s^*\right)_x=(J_s)_x\frac{\sigma_0^2}{\sigma_{xx}\sqrt{\sigma_{yy}\sigma_{zz}}},\left(J_s^*\right)_y=(J_s)_y\frac{\sigma_0^2}{\sigma_{yy}\sqrt{\sigma_{xx}\sigma_{zz}}},\left(J_s^*\right)_z=(J_s)_z\frac{\sigma_0^2}{\sigma_{zz}\sqrt{\sigma_{xx}\sigma_{yy}}} \quad \text{(Equation 8)}$$

where σ_0 is an arbitrary conductivity. Introducing Equations 7 and 8 into v_k yields:

$$\sigma_0(\nabla^*)^2\cdot V=\nabla^*\cdot\boldsymbol{J}^* \quad \text{(Equation 9)}$$

Equation 9 is the same as the potential field for a homogeneous volume, which its solution for a monopolar current source in an infinite domain is well known (Plonsey and Barr, 2007):

$$V^*(x^*,y^*,z^*)=\frac{I_0}{4\pi\sigma_0}\frac{1}{\sqrt{(x^*)^2+(y^*)^2+(z^*)^2}} \quad \text{(Equation 10)}$$

Converting back to dimensional variables, we obtained the potential field for a monopole current source I_0 located at (x_s, y_s, z_s) in the anisotropic volume as:

$$V(x,y,z)=\frac{I_0}{4\pi\sqrt{\sigma_{xx}\sigma_{yy}\sigma_{zz}}}\frac{1}{\sqrt{\frac{(x-x_s)^2}{\sigma_{xx}}+\frac{(y-y_s)^2}{\sigma_{yy}}+\frac{(z-z_s)^2}{\sigma_{zz}}}} \quad \text{(Equation 11)}$$

We used Equation 11 to calculate V_1 and V_2 in Equation 1. Assuming that the axon was positioned parallel to the x-axis, we used $\sigma_{xx}=0.6\ S/m$ and $\sigma_{yy}=\sigma_{zz}=0.083\ S/m$ to account for higher conductivity of white matter in the longitudinal direction compared to the transverse direction (Capogrosso et al., 2013; Foster and Schwan, 1989; Ranck and BeMent, 1965).

Amplitude Modulation (AM) and Beat Frequency

We used Euler's formula to write Equation 1 as:

$$V_1e^{i2\pi f_1t}+V_2e^{i2\pi f_2t}=e^{i2\pi\frac{f_1+f_2}{2}t}\left[V_1e^{i2\pi\frac{f_1-f_2}{2}t}+V_2e^{-i2\pi\frac{f_1-f_2}{2}t}\right] \quad \text{(Equation 12)}$$

where $i=\sqrt{-1}$. Equation 12 corresponds to a net field that oscillates with the average frequency of $(f_1+f_2)/2$, whereas its strength follows an envelope that oscillates with the frequency of f_1-f_2, also known as the beat frequency.

In the TI method, both the f_1 and f_2 frequencies are large, but the difference between them (i.e. beat frequency) is small, which results in an envelope that oscillates slowly while the net field itself is still oscillating with a high frequency. To find the time evolution of the envelope for the potential field, we multiplied Equation 12 by its conjugate to obtain:

$$|Env_V(t)|=\sqrt{V_1^2+V_2^2+2V_1V_2\cos(2\pi(f_1-f_2)t)} \quad \text{(Equation 13)}$$

The cosine term in Equation 13 varies between +1 and -1. Therefore, the envelope of the net field oscillates between $\sqrt{(V_1+V_2)^2}$ and $\sqrt{(V_1-V_2)^2}$ at a frequency of f_1-f_2. Hence, amplitude modulation (AM), which is the difference between the maximum and minimum of the field, can be stated as:

$$AM_V=||V_1+V_2|-|V_1-V_2|| \quad \text{(Equation 14)}$$

We can also define AM for the electric field in any direction. For example, AM in the x-direction can be stated as:

$$AM_{E_x}=||E_{x1}+E_{x2}|-|E_{x1}-E_{x2}|| \quad \text{(Equation 15)}$$

where E_{x1} and E_{x2} are the electric fields generated by the first and second electrode pairs, respectively. Note, we computed the electric fields by taking the gradient of Equation 11. We also calculated AM of the activating function (Rattay, 1986) in the x-direction:

$$AM_{A_x}=||A_{x1}+A_{x2}|-|A_{x1}-A_{x2}|| \quad \text{(Equation 16)}$$

where A_{x1} and A_{x2} are the activating functions of the fields generated by the first and second electrode pairs, respectively. The activating function is defined as the gradient of the electric field (Rattay, 1986).

Myelinated Axon Model

Axons and axon terminals have been shown to have the lowest threshold to invasive and non-invasive extracellular electrical stimulation (Aberra et al., 2018; Chakraborty et al., 2018; Howell and McIntyre, 2020; McIntyre et al., 2004; Rahman et al., 2013; Wongsarnpigoon and Grill, 2012). And because TI stimulation has been proposed as a potential non-invasive alternative to deep brain stimulation (i.e. suprathreshold stimulation) (Grossman et al., 2017), we modified a previously published compartmental model of a myelinated mammalian axon (McIntyre et al., 2002) to assess the axonal response to TI stimulation. This myelinated axon model includes active nodes of Ranvier and passive internode regions. In the original model, both the backward and forward rates for the slow potassium channel increase with the membrane potential. With such kinetics, the time constant of the channel changes monotonically and goes to infinity for large depolarizations. Moreover, the steady-state activation profiles of the original potassium channel indicate opening of the potassium channel during large hyperpolarization. These ion channel dynamics conflict with known physical principles that govern ion channels (Hille, 2001), and, to our knowledge, they have not been reported experimentally. Therefore, we adjusted the functional form of the kinetics for the slow potassium channel. Our modified axon model was able to reproduce experimental results, such as action potential and afterpotential shape, axonal excitability and the recovery cycle, impulse-dependent afterhyperpolarization, and spike frequency adaptation.

Morphology

We used the same morphology as the original compartmental model of a myelinated mammalian axon for diameters of 5.7 – 16.0 um (McIntyre et al., 2002) and a subsequent study for an axon diameter of 2.0 μm (McIntyre et al., 2004). The model morphology accounts for various sections of myelin along the internode by including myelin attachment segment (MYSA), paranode main segment (FLUT), and internode segment (STIN) regions of the fiber. Because the nervous system consists of axons with a wide range of diameters (Benavides-Piccione et al., 2020; Feirabend et al., 2002; Terao et al., 1994; Ugrenović et al., 2016), we investigated the axonal response to TI stimulation for a range of fiber sizes (Figure S5). We performed simulations for the following fiber diameters: 2.0, 3.0, 5.7, 8.7, 11.5, and 16.0 μm. Unless otherwise noted, we simulated axons with a diameter of 8.7 μm and a length of 100 mm.

Ionic Currents

At the nodes of Ranvier, the model included fast sodium (I_{Naf}), persistent sodium (I_{Nap}), slow potassium (I_{Ks}), leakage (I_L), and capacitive (I_C) currents:

$$I_{total} = I_{Naf} + I_{Nap} + I_{Ks} + I_L + I_C \quad \text{(Equation 17)}$$

We used the Hodgkin-Huxley formalism to model ionic currents:

$$I_{ion} = g_{ion}(V_m - E_{ion}) \quad \text{(Equation 18)}$$

where E_{ion} is the reversal potential, and g_{ion} is the conductance for the ion. The maximum conductance for the leak current ($\overline{g}_L$) is constant, but the conductance for the other currents can be written in terms of their gating variables:

$$g_{Naf} = \overline{g}_{Naf} m^3 h \quad \text{(Equation 19)}$$

$$g_{Nap} = \overline{g} m_p^3 \quad \text{(Equation 20)}$$

$$g_{Ks} = \overline{g}_{Ks} s \quad \text{(Equation 21)}$$

where m and h represent activation and inactivation variables of the fast sodium channel, respectively. m_p is the activation variable of the persistent sodium channel and s is the activation variable of the slow potassium channel. $\overline{g}_{Naf}$ is the maximum conductance of the fast sodium channel, $\overline{g}_{Nap}$ is the maximum conductance of the persistent sodium channel, and $\overline{g}_{Ks}$ is the maximum conductance of the slow potassium channel. The table below summarizes the reversal potentials and maximum conductances in our model.

Current	Reversal Potential [mV]	Maximum Conductance [S/cm^2]
Fast sodium (*Naf*)	50	3.0
Persistent sodium (*Nap*)	50	0.01
Slow potassium (*Ks*)	-90	0.08
Leakage (*L*)	-90	0.007

All of the gating variables followed first-order dynamics:

$$\frac{dX}{dt} = \alpha_X(V_m)(1-X) - \beta_X(V_m)X \quad \text{(Equation 22)}$$

where $\alpha_X(V)$ was the voltage-dependent forward rate and β_X(V) was the voltage-dependent backward rate for the gating variable. We used the following general forms for the rate constants:

$$\alpha_m, \alpha_{mp}, \alpha_s = \frac{A(V_m+B)}{1-e^{-\frac{V_m+B}{C}}} \quad \text{(Equation 23)}$$

$$\alpha_h, \beta_m, \beta_{mp}, \beta_s = \frac{-A(V_m+B)}{1-e^{\frac{V_m+B}{C}}} \quad \text{(Equation 24)}$$

$$\beta_h = \frac{A}{1-e^{-\frac{V_m+B}{C}}} \quad \text{(Equation 25)}$$

The table below summarizes all of the constants necessary to model the ionic currents for 20°C.

	Constants			
Rates	A [ms^{-1}]	B [mV]	C [mV]	Q_{10}
α_m	1.85	21.4	10.3	2.2
α_h	0.034	112	11	2.9
α_{mp}	0.03	23	10.2	2.2
α_s	0.0138	14	9.4	3.0
β_m	0.076	25.7	9.16	2.2
β_h	2.3	28.8	13.6	2.9
β_{mp}	0.00019	38	10	2.2
β_s	0.000138	56	1	3.0

The time constant (τ_X) and steady-state activation (X_∞) for a gating variable X is defined as:

$$\tau_X(V_m) = \frac{1}{\alpha_X(V_m)+\beta_X(V_m)}, X_\infty(V_m) = \frac{\alpha_X(V_m)}{\alpha_X(V_m)+\beta_X(V_m)} \quad \text{(Equation 26)}$$

We changed α_x and β_x by the same amount (δ) to alter time constants for different ion channels:

$$\tau_X^{new}(V_m) = \frac{1}{\delta\alpha_X(V_m)+\delta\beta_X(V_m)} \quad \text{(Equation 27)}$$

Then, we found δ that enforces the desired relative change in the time constant. For example, to increase the time constant by 25% we have:

$$\frac{\tau_X^{new}(V_m)-\tau_X^{old}(V_m)}{\tau_X^{old}(V_m)} = 0.25 \Rightarrow \frac{1}{\delta} - 1 = 0.25 \Rightarrow \delta = \frac{4}{5} \quad \text{(Equation 28)}$$

Note that changing the forward and backward rates by the same amount keeps the steady-state activation unchanged:

$$X_\infty^{new}(V_m) = \frac{\delta\alpha_X(V_m)}{\delta\alpha_X(V_m)+\delta\beta_X(V_m)} = \frac{\alpha_X(V_m)}{\alpha_X(V_m)+\beta_X(V_m)} = X_\infty(V_m) \quad \text{(Equation 29)}$$

It should be noted that the optimum TI frequency changed during the sensitivity analysis when we varied the time constants of the gating variable. The optimum TI frequency depends heavily on the time constant of the potassium channel, which is known to affect resonance properties of neurons (Hutcheon and Yarom, 2000). Indeed, during the sensitivity analysis (Figures 6 and S4), -50%, -25%, +25% and +50% change in the potassium channel time constant (τ_s) changes the optimum beat frequency from 5 Hz to 10 Hz, 6Hz, 4 Hz, and 3 Hz, respectively. These results are consistent with where resonance is expected to occur (between $1/2\pi\tau_s$ and $1/2\pi\tau_{membrane}$) (Hutcheon and Yarom, 2000). Moreover, the frequency range for our axon model is in line with values reported in the literature for somata of different neurons. For example, rat hippocampal neurons show a wide range of resonance frequencies roughly between 1-12 Hz (Hu et al., 2009; Narayanan and Johnston, 2007). Also, a resonance frequency of 2 Hz has

been reported for layer 5 neocortical pyramidal neurons (Dwyer et al., 2012) and neocortical layer 2–3 pyramidal neurons have been shown to have resonance frequencies in the range of 3-12 Hz (Higgs and Spain, 2009). Moreover, changing the time constant resulted in changes in the activation threshold. Hence, for the sensitivity analysis, in addition to using the optimum beat frequency, we used the activation threshold for each set of new parameters (Figures 6C, 6D, S3, and S4).

Model Implementation

To calculate the response of myelinated axons to extracellular TI stimulation, we used the NEURON simulation software (v7.7) with the Python programming language (Hines and Carnevale, 1997; Hines et al., 2009). At each time step and at the center location of each axon compartment, we calculated the total extracellular voltage from the TI stimulation using Equations 1 and 11. We applied these voltages to the axons using NEURON's extracellular mechanism. We calculated the model solutions using NEURON's backward Euler implicit integration method with a fixed time step of 5 μs. We ran simulations for a total duration of ten beats and defined the activation threshold as the minimum current that resulted in at least a single action potential during each beat. To find the activation thresholds, we used a binary search with a relative error of 0.1%. We used carrier frequencies of 1, 2, and 4 kHz and tested for beat frequencies of 1-50 Hz in steps of 1 Hz. We assessed both the effects of TI stimulation at the axon terminal (by placing the end node, Node 100, at x=0 mm) and stimulation near the middle of the axon (by placing the center node, Node 50, at x=0 mm).

We also assessed the influence of boundary conditions, which can affect the transmembrane voltage solutions near axon terminals (Rubinstein, 1993; Wongsarnpigoon and Grill, 2012). We utilized the standard "sealed end" boundary condition in which all of the current at the terminal nodes of Ranvier flowed through the radial membrane sections (axial current was zero) (Rubinstein, 1993; Tranchina and Nicholson, 1986). To assess the effect of this boundary condition, we increased the surface area of the terminal nodes to include the membrane at the very end of the cylindrical compartment. We also ran simulations in which we removed active properties from the terminal nodes so that they only contained passive properties. We then assessed the changes in our model predictions by performing the same analysis described in Figure 6 for TI stimulation applied using a 2 kHz carrier frequency and a 5 Hz beat frequency. For stimulation applied near the end of the axon (Node 100 at x=0 mm), we observed a 18.7% decrease and a 135% increase in the activation thresholds for the increased surface area nodes and passive nodes, respectively. We observed no changes in the activation thresholds for stimulation applied near the middle of the axon (Node 50 at x=0 mm). Although, we did observe significant changes in the stimulation thresholds, the qualitative trends were similar for all terminal conditions in which we still observed the "sandwich" response pattern (data not shown). Because the axon terminals are highly excitable, additional experimental work is necessary to characterize the geometric and electrical properties of axon terminals and how these properties influence the neural response to extracellular electrical stimulation (Wongsarnpigoon and Grill, 2012).